scientific reports

Check for updates

OPEN

Integrative pan-cancer analysis and experiment validation identified GLS as a biomarker in tumor progression, prognosis, immune microenvironment, and immunotherapy

Dongming Li[1], Donghui Cao[2], Yangyu Zhang[2], Xinyi Yu[2], Yanhua Wu[2], Zhifang Jia[2], Jing Jiang[2]✉ & Xueyuan Cao[1]✉

Glutaminase (GLS), a crucial gene regulating glutaminolysis, has received much attention as it was found to regulate tumor metabolism and copper-induced cell death. However, its biological roles and mechanisms in human cancers remain obscure. Consequently, the integrated pan-cancer analyses and biological experiments were conducted to elucidate its oncological functions. We found GLS was differentially expressed in human cancers and upregulated GLS predicted poor survival, clinicopathological progression, and tumor heterogeneity. Single-cell analysis found GLS was closely related to various biological functions and pathways. Spatial transcriptomic analysis found GLS expression was mainly derived from tumor cells, which implies tumor cells may have a stronger ability to utilize glutamine than antitumor immune cells in the tumor microenvironment (TME). Meanwhile, we noticed GLS expression was strongly related to the infiltration of various immune cells and stromal cells, the expression of immunomodulatory genes, the activity of some conventional antitumor agents, and the therapeutic response of immunotherapy. Moreover, enrichment analyses suggested GLS was related to various metabolic reprogramming, innate and adaptive immunity suppression, and extracellular matrix remodeling. Finally, we observed GLS was highly expressed in our gastric cancer (GC) cohort. As an independent risk factor for GC prognosis, high-GLS was closely related to pathological progression. Inhibiting GLS expression in GC cells effectively prevented proliferation, migration, and invasion and triggered apoptosis. In conclusion, GLS is an underlying biomarker for oncological progression, prognosis, TME, antitumor drug sensitivity, and immunotherapy response. Targeting GLS can facilitate the implementation of individualized and combined treatment strategies.

Keywords GLS, Pan-cancer analysis, Gastric cancer, Biomarker, Tumor microenvironment, Immunotherapy

Globally, cancer has been recognized as a leading cause of death, as its incidence and mortality are rising quickly[1]. The aberrant alternations of cancer-associated genes drive the complex process of tumorigenesis, progression, and evolution, resulting in significant heterogeneity and poor prognosis, which remains considerable challenges for tumor treatment[2–4]. Immunotherapy has made remarkable progress and has become a key therapeutic strategy for multiple tumors in recent years, whereas only subsets of tumor patients benefit from it[5]. Consequently, it is extremely indispensable to seek potential genetic biomarkers for predicting which patients may be suitable for immunotherapy.

In addition to glucose metabolism, uncontrolled glutamine metabolism is another crucial prerequisite for tumor biosynthesis and energy supply[6]. Specifically, glutamine is a pivotal carbon pool and nitrogen pool for malignant cells, and its catabolism provides precursors for the biosynthesis of nucleotides and non-essential

[1]Department of Gastric and Colorectal Surgery, General Surgery Center, The First Hospital of Jilin University, Changchun 130021, Jilin, China. [2]Department of Clinical Epidemiology, The First Hospital of Jilin University, Changchun 130021, Jilin, China. ✉email: jiangjing19702000@jlu.edu.cn; jd3d2ub@jlu.edu.cn

amino acids, thereby facilitating the proliferation and division of tumor cells[7–9]. Besides, glutamine participates in the generation of glutathione and nicotinamide adenine dinucleotide phosphate to maintain cellular redox balance, thereby creating a favorable microenvironment for cellular malignant transformation and survival[10,11]. Moreover, due to the decreased flux of oxidative phosphorylation in tumor cells resulted from the Warburg effect, glutamine endlessly supplies tricarboxylic acid (TCA) cycle intermediates α-ketoglutarate to replenish the energy expenditure needed for sustained proliferation[12,13]. Briefly, tumor cells can reprogram aforementioned glutamine metabolism pathways to support their energy requirement and biosynthesis.

Glutaminase (GLS), a crucial regulator of glutamine metabolism, is responsible for hydrolyzing glutamine to glutamate and ammonia[14]. Physiologically, GLS expression is primarily concentrated in the kidney and brain tissues, involved in cellular energy metabolism, cerebral neurotransmitter synthesis, and renal acid-base maintenance[15,16]. However, GLS expression is often dysregulated in malignant cells as metabolic reprogramming occurs. Its dysregulation continuously drives glutaminolysis for the complement of TCA cycle and biosynthetic consumption, assisting malignant tumors to spread wildly. Therefore, targeting GLS-mediated glutamine metabolism to deprive the glutamine utilization of tumor cells is promising as a therapeutic strategy for cancer, which has received extensive attention. Remarkably, a recent study has reported GLS, as a cuproptosis-related gene, negatively regulates copper-triggered cell death[17]. Since this novel cell death pattern may be involved in the tumorigenesis and progression, it once again arouses academic interest in GLS research. Although GLS is recognized to drive tumorigenesis, the detailed roles of GLS in prognostic outcome, tumor microenvironment (TME), immunoregulation, and immunotherapy still need to be systematically investigated based on multi-omics analyses.

In this research, a systematic pan-cancer analysis was performed to mainly elucidate the association of GLS with tumor progression, prognosis, single-cell function, genetic alteration, antitumor drug sensitivity, immune microenvironment, and immunotherapy response, aiming to clarify its biological functions in human tumors and provide a reference for decision-making of individualized and combined antitumor therapies. In addition, we validated its expressed differences in gastric cancer (GC) as well as its potential roles in tumor progression and prognosis using a clinical GC cohort and in vitro biological experiments. Briefly, we found GLS is an underlying prognostic, therapeutic, and immunological biomarker in human cancers.

Materials and methods

Data collection

Transcriptomic datasets of 33 cancer types and their matching clinical data were derived from The Cancer Genome Atlas (TCGA) (https://portal.gdc.cancer.gov), Genotype-Tissue Expression (GTEx) (https://gtexportal.org), and Therapeutically Applicable Research to Generate Effective Treatments (TARGET) (https://ocg.cancer.gov/programs/target) databases. The transcript of GLS in each sample was extracted and $\log_2(TPM+1)$ transformation was performed in these transcriptomic profiles. The abbreviations and expanded names of 33 tumor types are displayed in Table 1. The samples derived from tumor tissues and corresponding normal tissues were included for further pan-cancer analysis but the samples with missing gene expression or lacking required clinical information were eliminated. The proteomics datasets of GLS were derived from the Clinical Proteomic Tumor Analysis Consortium (CPTAC) (https://pdc.cancer.gov/pdc/) and all proteomic expression values were converted into unitless Z-scores. Furthermore, the single-cell spatial transcriptome datasets were acquired from the Gene Expression Omnibus (GEO) (https://www.ncbi.nlm.nih.gov/geo/) and 10x Genomics (https://www.10xgenomics.com/) databases. The workflow in this study is demonstrated in Fig. 1.

Differential expression analysis

The mRNA expression of GLS between tumor and normal tissues was compared in TCGA samples with or without matched GTEx data across 33 tumor types. The co-expression correlation analysis across TCGA tumors was performed to clarify the correlation between GLS and the remaining 9 confirmed cuproptosis-related genes (CRGs). Furthermore, we investigated the total protein levels of GLS utilizing the CPTAC samples, and Wilcoxon rank sum tests were selected to compare protein expression differences between different groups. Lastly, the immunohistochemical (IHC) staining images were acquired to supplement and validate the GLS protein expression in different tissues through inquiring about the Human Protein Atlas (HPA) (https://www.proteinatlas.org/) database, in which the quantity of stained cells (including not detected, $<25\%$, 25–75% and $>75\%$) and staining intensity (including negative, weak, moderate, and strong) were used to assess the expression levels of GLS protein.

Association between GLS expression and clinical characteristics

The relevance of GLS expression to distinct clinical features was investigated. We further detected the expression difference of GLS across the different demographic and oncological characteristics, including gender, age, pathological TNM stage, and histological grade across TCGA tumor samples. Furthermore, the "Gene expression comparison" module in TNMplot (https://tnmplot.com/analysis/) was manipulated to analyze whether GLS expression was associated with tumor metastasis. The differential levels of GLS among normal, tumor, and metastatic samples were compared based on the RNA-Seq data and gene chip data. Differential expression analyses were measured via the Kruskal-Wallis test with a post-hoc Dunn's test or One-way ANOVA with a post-hoc Tukey Honestly Significant Difference test when appropriate.

Survival analysis

We selected the overall survival (OS), disease-free interval (DFI), and progression-free interval (PFI) to assess the potential impact of GLS expression on survival outcomes. After excluding the patients with follow-up time or survival time less than thirty days, the potential prognostic role of GLS expression in TCGA and TARGET

Number	Tumor types	Abbreviations
1	Adrenocortical carcinoma	ACC
2	Bladder urothelial carcinoma	BLCA
3	Breast invasive carcinoma	BRCA
4	Cervical squamous cell carcinoma and endocervical adenocarcinoma	CESC
5	Cholangiocarcinoma	CHOL
6	Colon adenocarcinoma	COAD
7	Lymphoid neoplasm diffuse large B-cell lymphoma	DLBC
8	Esophageal carcinoma	ESCA
9	Glioblastoma multiforme	GBM
10	Head and neck squamous cell carcinoma	HNSC
11	Kidney chromophobe	KICH
12	Kidney renal clear cell carcinoma	KIRC
13	Kidney renal papillary cell carcinoma	KIRP
14	Acute myeloid leukemia	LAML
15	Brain lower grade glioma	LGG
16	Liver hepatocellular carcinoma	LIHC
17	Lung adenocarcinoma	LUAD
18	Lung squamous cell carcinoma	LUSC
19	Mesothelioma	MESO
20	Ovarian serous cystadenocarcinoma	OV
21	Pancreatic adenocarcinoma	PAAD
22	Pheochromocytoma and paraganglioma	PCPG
23	Prostate adenocarcinoma	PRAD
24	Rectum adenocarcinoma	READ
25	Sarcoma	SARC
26	Skin cutaneous melanoma	SKCM
27	Stomach adenocarcinoma	STAD
28	Testicular germ cell tumors	TGCT
29	Thyroid carcinoma	THCA
30	Thymoma	THYM
31	Uterine corpus endometrial carcinoma	UCEC
32	Uterine carcinosarcoma	UCS
33	Uveal melanoma	UVM

Table 1. The expanded names and abbreviations of 33 tumor types.

cohorts was analyzed. The "maxstat (v.0.7.25)" R package was utilized to calculate the optimal cutoff value of the GLS expression. The "survival (v.3.3.1)" and "survminer (v.0.4.9)" R packages were applied to analyze prognostic differences. The Kaplan-Meier (K-M) survival curves were delineated in diverse GLS expression subgroups and Cox regression was performed to determine whether these survival curves were significant. Additionally, the "K-M plotter" module in Kaplan-Meier Plotter (https://kmplot.com/analysis/) was manipulated as a supplement to illuminate its prognostic effects on tumor patients.

Single-cell analysis and spatial transcriptomic atlas

Single-cell sequencing technology has become a crucial tool to explore tumor progression, heterogeneity, and therapeutic response. We dissected the tumor single-cell sequencing data to examine the relationship between GLS expression and 14 single-cell functional states across multiple tumor types via the CancerSEA (http://biocc.hrbmu.edu.cn/CancerSEA/) platform, where the gene set variation analysis (GSVA) and Spearman's correlation were employed separately to calculate the tumor single-cell functions and the correlation between these functions and GLS expression. The functional states with the most significance ($p < 0.001$) and corresponding expression distribution diagrams were also simultaneously obtained in specific single-cell samples in the CancerSEA database. With no STAD data available in the CancerSEA database, it was necessary to further elaborate on the biological roles of GLS in STAD. Hence, we acquired a single-cell transcriptome dataset (GSE167297), which included 41,554 cells, downloaded from the TISCH (http://tisch.comp-genomics.org/) database. To identify clusters and patterns in the STAD dataset, we applied the Uniform Manifold Approximation and Projection (UMAP) method to visualize high-dimensional data as a two-dimensional heatmap, and to visualize GLS expression at single-cell resolution. Meanwhile, the Kruskal-Wallis test was utilized to compare its biological expression among different cell types. According to whether these cells expressed GLS or not, we divided them into the GLS-positive expression group and GLS-negative expression group and calculated the proportion of each cell type in the two groups respectively. To evaluate the biological effects of GLS expression on tumor

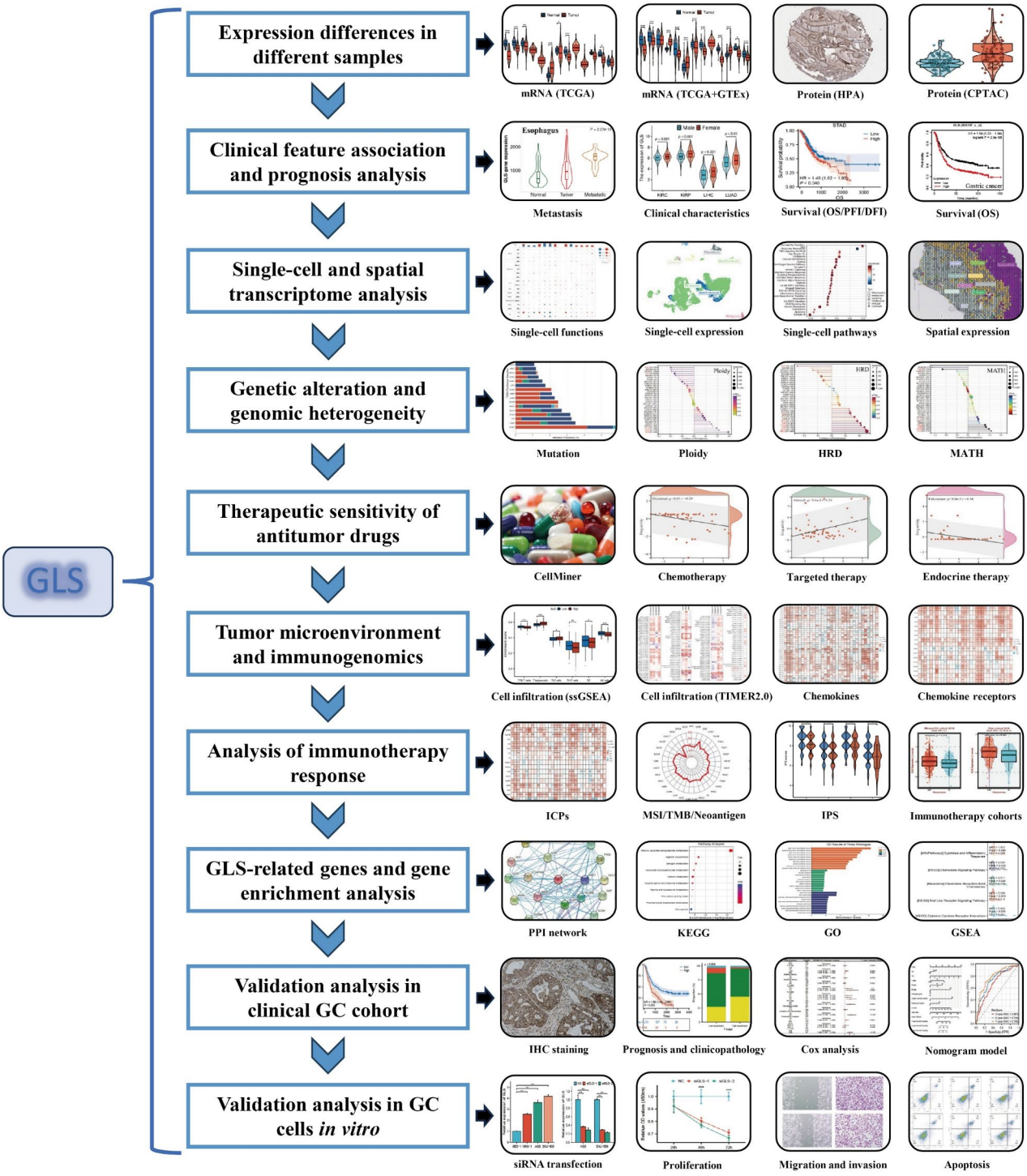

Fig. 1. Diagram of main workflow in this study.

cells, various biological pathways related to immunity, metabolism, mitochondria, cell death, proliferation, and signaling were enriched in malignant tumor cells using the "AUCell (v.1.26.0)" R package and the referenced Hallmark and MitoCarta3.0 gene sets[18,19]. The differences in pathway scores between the two groups of malignant tumor cells were compared via the "limma (v.3.60.0)" R package.

Single-cell spatial transcriptome samples were obtained from the GEO (GSE203612, GSE175540, and GSE179572) and 10x Genomics databases. Detailed sample sources are provided in **Table S1**. To accurately identify the cell composition in each spot on the slides, deconvolution analysis was performed based on the referenced scRNA-seq data. Firstly, we constructed a signature matrix by calculating the average expression of specific expression genes for each cell type in each spot. Next, based on the "get_enrichment_matrix" and

"enrichment_analysis" functions in the "Cottrazm (v.1.0.0)" R package, we generated the enrichment score matrix for cell composition identification. Then, the most abundant cell type and GLS expression landscape in each spot were calculated and visualized utilizing the "SpatialDimPlot" and SpatialFeaturePlot" functions in the "Seurat (v.5.0.3)" R package. Furthermore, a malignant spot was defined if its cells were exclusively malignant, and a normal spot was defined if its cells were exclusively non-malignant. Otherwise, the mixed malignant spot was defined. Wilcoxon rank sum tests were utilized to assess statistical differences in GLS expression between the two groups.

Landscapes of genetic alteration and genomic heterogeneity

The cBioPortal (https://www.cbioportal.org/) was manipulated to elucidate the genetic alteration across the TCGA tumors, involved in genetic mutation, amplification, structural variant, and deep deletion, based on the "Query" searching module and "TCGA PanCancer Atlas Studies" datasets. Then the "Immune-Mutation" module in TIMER2.0 (http://timer.cistrome.org/) was utilized to clarify the association of the GLS mutation with multiple immune cell infiltration. Lastly, to delineate whether genomic heterogeneity was relevant to GLS expression, we analyzed chromosome ploidy, homologous recombination deficiency (HRD), and mutant-allele tumor heterogeneity (MATH) based on the Sangerbox3.0 platform (http://vip.sangerbox.com/), in which the ploidy and HRD data were derived from a previous study[20], and MATH scores were calculated using the simple nucleotide variation datasets across TCGA tumor samples from TCGA portal based on the "inferHeterogeneity" function of "maftools (v.2.8.5)" R package.

Analysis of antitumor drug sensitivity

To uncover the association of GLS expression with antitumor drug sensitivity, we retrieved the pharmacogenomic datasets by searching the CellMiner database (https://discover.nci.nih.gov/cellminer/home.do). The classic NCI-60 cancer cell line was selected for cytotoxic screening of antitumor compounds in vitro[21]. The drug activities for chemotherapies, targeted therapies, and endocrine therapies with Food and Drug Administration (FDA) approval were examined to search for potential antitumor therapeutic agents. Correlation analysis was performed between GLS mRNA expression (Z-value) and drug activity.

Analysis of tumor immune microenvironment

To investigate the association of GLS expression with tumor immune microenvironment, we performed a Single-sample Gene Set Enrichment Analysis (ssGSEA) algorithm for various immune cell infiltration analyses in TCGA tumor samples. Based on markers for various immune cells reported in previous literature, the "GSVA (v.1.46.0)" R package was applied to perform the ssGSEA analysis[22]. B cells, T cells, dendritic cells (DCs), eosinophils, mast cells, natural killer (NK) cells, macrophages, neutrophils, and cytotoxic cells were selected to analyze their infiltration levels. Additionally, the "Immune-Gene" module in TIMER2.0 was manipulated to explore the association between GLS expression and various infiltrated cells in the TME. $CD4^+$ T lymphocytes, $CD8^+$ T lymphocytes, cancer-associated fibroblasts (CAFs), endothelial cells (ECs), regulatory T cells (Tregs), and myeloid-derived suppressor cells (MDSCs) were filtrated for further correlation analysis. The default immune deconvolution methods in TIMER2.0 were utilized to calculate the infiltration abundances of various cells.

Analysis of immunogenomics and immunotherapeutic response

Immune checkpoints (ICPs), as immune regulators, act a pivotal part in maintaining tumor immune microenvironment. Targeting ICPs remains an especially considerable immunotherapy modality today. We acquired an immunomodulatory gene list from a previous study that included 24 inhibitory checkpoints[20]. The co-expression connections between GLS expression and these immunomodulatory checkpoints were analyzed across TGCA tumors through correlation analysis. Furthermore, in malignant tumors, the dysregulated chemokines as well as their receptors can change immune cell recruitment and activation, often towards a tumorigenic state, which has become a potential target for tumor immunotherapy[23–25]. Thus, correlation analyses were performed to examine whether GLS expression was relevant to chemokines and their receptors across various TGGA cancer types.

To illustrate the roles of GLS in immunotherapy, several tumor immunogenicity predictors, including microsatellite instability (MSI), tumor mutational burden (TMB), and tumor neoantigen that were acquired from Sangerbox3.0 platform, were selected to estimate the immunotherapeutic response in TCGA tumors. The radar map visualized the correlations between GLS expression and MSI, TMB, and tumor neoantigen. Since immunophenoscore (IPS) is a well-established and remarkable predictor of immunotherapy response, we categorized the TCGA tumor patients into different subgroups based on the GLS expression median and compared the IPS levels between the different subgroups. The IPS scores in TCGA samples were acquired from the TCIA (https://tcia.at/home) database. A higher IPS score implies a more sensitive response to immunotherapy. Additionally, two independent immunotherapy cohorts (IMvigor210 and GSE91061) in the GEO database were retrieved to validate the potential effect of GLS on tumor immunotherapy. The patients who developed complete or partial responses after immune checkpoint inhibitor (ICI) treatment were identified as immunotherapeutic responders and those who developed stable or progressive diseases were identified as non-responders. The differences in GLS expression between the responders and non-responders were explored, and relevant immunotherapeutic survival curves were obtained via the "Start KM Plotter for immunotherapy" module in the Kaplan-Meier Plotter database to infer immunotherapeutic prognosis in different GLS expression subgroups.

GLS-related gene enrichment analysis

The STRING (https://cn.string-db.org/) was manipulated to acquire the top 20 interactors relevant to GLS based on the protein-protein interaction (PPI) network. "Full STRING network" was chosen in the settings options and active interaction sources were limited to "experiments" and "databases". Meanwhile, the "Correlation Analysis" module in the GEPIA2 (http://gepia2.cancer-pku.cn/) platform was utilized to obtain the top 100 similar genes of GLS through Pearson correlation analysis. Whereafter, a correlation heatmap of the selected genes was delineated across TCGA tumors to supply the correlativity between GLS and GLS-related genes utilizing the "Exploration- Gene_Corr" module of the TIMER2.0 platform. To discover the influence of GLS on pathways and biological processes, the Kyoto Encyclopedia of Genes and Genomes (KEGG) and Gene Ontology (GO) enrichment analysis were performed using the aforementioned 120 genes based on the "clusterProfiler (v.4.4.4)" R package.

After that, we classified the TCGA tumor samples into different expression subgroups based on the GLS expression median. With $|\text{LogFC}|>1.0$ and adjusted $p<0.05$ as the threshold value, the differential expression genes between the two subgroups were calculated via the "DESeq2 (v.1.36.0)" R package. The Gene Set Enrichment Analysis (GSEA) analysis subsequently was conducted via the "clusterProfiler" R package utilizing the differentially expressed genes in different TCGA tumor types.

Gastric cancer population

We collected the clinical information of 295 patients who were pathologically diagnosed with GC at the Department of Gastrointestinal Surgery of the First Hospital of Jilin University from January 2011 to December 2016. All enrolled patients underwent gastric surgery but did not undergo preoperative neoadjuvant chemoradiotherapy. We extracted clinical information of these GC patients, such as age, sex, body mass index, smoking history, drinking history, pathological TNM stages (AJCC 8th), histological grades, lympho-vascular invasion, perineurium invasion, and MSI, from the hospital's medical record system. The clinical information regarding these GC samples is summarized in **Table S2**. The data collection and further study were approved by the Ethics Committee of the First Hospital of Jilin University (No.2021 − 493) and relevant informed consent was obtained. Regular follow-up was performed in accordance with our previous study[26]. All follow-up works were completed until August 2022 and OS for each patient was calculated separately during follow-up.

Immunohistochemical staining and scoring

In the above GC population, 295 tumor tissues and 277 paired para-tumor tissues were acquired for IHC staining. Briefly, the paraffin sections were baked at 65 °C for 30 min, followed by dewaxing and rehydration. After repairing the antigen with sodium citrate (MVS-0101, Maixim, China), the sections were placed in a wet box and an endogenous peroxidase blocker (SP KIT-A3, Maixim, China) was added. Subsequently, normal non-immune goat serum (SP KIT-B2 Maixim, China) was added for antigen blocking. Then, the tissue sections were incubated with GLS monoclonal antibody (#56750, CST, USA) overnight at 4℃, followed by a secondary antibody (KIT-5020, Maixim, China) for 30 min. After color detection with 3,3-diaminobenzidine tetrahydrochloride (DAB-1031, Maixim, China), re-staining with hematoxylin and differentiation with hydrochloric alcohol were carried out. Finally, the tissue sections were dehydrated and mounted.

The ASI system (Applied Spectral Imaging Ltd., Israel) was applied to estimate the staining intensity and the percentage of stained tumor cells in each tissue section. The staining intensity was classified as 0 (no staining), 1 (light yellow), 2 (light brown), or 3 (brown). According to the percentage of stained tumor cells (pi) and the staining intensity (i), the H-score (H-score $=\Sigma(pi\times i)$) was calculated to assess GLS protein expression levels in different tissues. Subsequently, differences in GLS expression between tumor tissues and para-tumor tissues were tested based on H-score. Based on the optimal cutoff value of the H-score, these patients were categorized into different expression subgroups, and the OS was simultaneously visualized utilizing "survival" and "survminer" R packages. Cox regression was performed to compute the hazard ratio (HR) for OS. The distribution of pathological features between the different subgroups was subsequently assessed using the Chi-squared test. After univariate and multivariate Cox regression analyses were performed using "survival" R package, the clinical nomograms based on or without GLS H-score were constructed via "survival" and "rms (v.6.3.0)" R packages to conveniently predict prognostic survival in GC patients. The 3-, 5-, and 7-year time-dependent ROC curves and calibration curves were plotted to evaluate the nomogram's predictive utility via "timeROC (v.0.4)", "survival", and "rms" R packages. Similarly, we plotted ROC curves for the clinical and pathological variables shown in the nomogram model to compare the difference in predictive accuracy between GLS-based risk model and these variables.

Cell culture and GLS targeted siRNA transfection

Immortalized gastric normal epithelial cell line GES-1 and GC cell lines, including AGS, MKN-1, and SNU-638, were provided by ZQXZbio (Shanghai, China) and Procell Life Science & Technology (Wuhan, China). These cells were cultured in RPMI-1640 medium with 10% fetal bovine serum (FBS) and 1% penicillin-streptomycin solution and placed in a 37℃-incubator containing 5% CO_2. Once the cell confluence reached 60–80% in culture plates, siNC or siGLS (GenePharma, China) was transfected into GC cells utilizing lipofectamine RNAiMAX (13778030, Invitrogen, USA) according to the manufacturer's instruction. The oligonucleotide sequences for siRNAs are displayed in **Table S3**. Briefly, Opti-MEM medium was used to dilute lipofectamine and siRNA (10μM), respectively. Subsequently, they were mixed and incubated at room temperature for 5 min to prepare the siRNA-liposomes that were then added to each well.

Quantitative real-time PCR (qPCR) assays

When GC cells were transfected for 48 h, we extracted cellular RNA using Molpure® Cell/Tissue Total RNA Kit (19221ES50, YEASEN, China). The concentrations of the extracted RNA were quantified utilizing a

NANODROP 2000c spectrophotometer (Thermo Scientific, USA). Subsequently, the reverse transcription process was performed in C1000™ Thermal Cycler (BIO-RAD, Singapore) device utilizing the ToloScript RT EasyMix for qPCR Kit (#22106, Tolo Biotech, China). All primers used for qPCR were synthesized following the sequence in **Table S4**. The qPCR reaction was performed utilizing the 2×Q3 SYBR qPCR Master Mix (#22204, Tolo Biotech, China) premixed solution and LightCycler® 480II Instrument (Roche, Switzerland). Additionally, differential expression of GLS mRNA between normal GES-1 and GC cells was also performed following the qPCR procedure described above.

Western blotting assays

Total protein of GC cells was extracted using RIPA Lysis Buffer (SL1010, CooLaber, China) and quantified using BCA Protein Assay Kit (ZJ101, Epizyme, China). Protein electrophoresis was performed using SDS-PAGE Gel Rapid Preparation Kit (PG112, Epizyme, China) and Tris-Gly buffer system. Subsequently, the proteins in the gel were transferred to the 0.45 μm pore size polyvinylidene fluoride (PVDF) membranes (IPVH00010, MILLIPORE, USA). After sealing with 5% skim milk for 2 h, the PVDF membranes were incubated overnight at 4℃ in anti-GLS antibody (#56750, CST, USA) and anti-β-Actin antibody (abs171598, Absin, China). The next day, the secondary antibody labeled with HRP (H6162, UElandy, China) was incubated at room temperature for binding to primary antibody. The ECL Femto Light Chemiluminescence Kit (SQ201, Epizyme, China) was used for chemiluminescence detection of protein bands.

Cell counting Kit-8 (CCK-8) assays

CCK-8 assays were applied to explore the role of GLS knockdown in GC cell proliferation. GC cells were evenly spread into 96-well plates with 1×10^4 cells per well and cultivated to the desired confluence. The cell viability was detected at 24 h, 48 h, and 72 h after siRNA transfection. 10 μl of CCK-8 (C6005, UElandy, China) solution was added to each well and incubated in the incubator sheltered from light for 1 h. Ultimately, the absorbance of each well was detected at 450 nm wavelength utilizing a microplate reader (Thermo Scientific, USA).

Wound healing assays

1×10^6 GC cells were spread into each well of 6-well plates after transfection. Once their confluence was close to 100%, the cell layer was scratched vertically utilizing the 200 μl pipette tip and photographed under a microscope immediately. After these GC cells were cultivated in an FBS-free medium for 48 h, the scratched sites were photographed again. The ImageJ (v.1.46r) software was utilized to calculate the cell migration distance between the corresponding photographs.

Transwell migration assays

After transfection for 24 h with serum-free culture, we seeded 1×10^5 GC cells into the upper chamber (3422, Corning, USA) with 200 μl of serum-free RPMI-1640 medium. Accordingly, we added 600 μl of medium containing 20% FBS into the lower transwell chamber. While GC cells were cultured for 24 h, we lightly wiped the GC cells in the upper chamber using cotton swabs, and then 4% paraformaldehyde was used to immobilize GC cells entering the lower chamber. Finally, the migrating cells were stained using 0.1% crystal violet. Five random microscopic fields were photographed and ImageJ software was used to estimate the cell number in each field.

Matrigel invasion assays

A 10-fold dilution of the Matrigel (356234, Corning, USA) was performed using a cold FBS-free medium. Next, we added 100 μl of diluted Matrigel into the upper transwell chamber and incubated in the incubator for at least 3 h to form a matrix film in the upper chamber. Subsequently, we seeded 1×10^5 transfected GC cells with 200 μl of FBS-free medium into the upper chamber. The subsequent operation was the same as the description in the transwell migration assay.

Cell apoptosis assays

GC cells were seeded into 6-well plates with 2×10^5 cells per well and cultivated for 24 h. Subsequently, these cells were transfected by siRNA and continued to be cultured for 48 h. The YF®488-Annexin V and PI Apoptosis Kit (Y6002, UElandy, China) was utilized to assess the cell apoptosis levels based on the manufacturer's instruction. In brief, GC cells were digested using EDTA-free trypsin and collected in the centrifuge tubes, then these cells were recovered in optimal cell culture conditions and medium for 30 min. Then they were washed twice using cold PBS and were re-suspended with Annexin V binding buffer. After being filtered by 40 μm cell screens, they were stained using YF®488-Annexin V and PI and incubated at room temperature for 15 min away from light. Ultimately, 200 μl of Annexin V binding buffer was supplemented before detecting the apoptosis via flow cytometry (BD, USA).

Statistical analysis

The normality of distribution and homogeneity of variance of continuous data were examined via the Shapiro-Wilk test and Levene's test, respectively, since they determined which statistical method was the optimal option. Wilcoxon rank-sum test or independent-sample T test was selected to test the statistical differences between two different subgroups. Similarly, Kruskal-Wallis test or One-way ANOVA was applied to analyze the significant differences among multiple subgroups. Subsequently, a post-hoc test was performed for pairwise comparisons by Dunn's test or Tukey Honestly Significant Difference test when appropriate. Wilcoxon signed-rank test was performed to test the statistical significance in paired samples. Correlation analyses were measured through the Spearman or Pearson test when appropriate. The K-M curves were delineated based on diverse GLS expression

subgroups categorized by the optimal cutoff value. Cox regression was performed to test the statistical differences in survival curves. Univariate and multivariate Cox regression analyses were applied to identify prognostic risk factors. Two-tailed $p < 0.05$ was considered statistically significant. The R software (v.4.2.0) was utilized for statistical analysis and the "ggplot2 (v.3.3.6)" R package was utilized to visualize analyzed data.

Results

GLS is abnormally expressed in human cancers

Through comparing transcription data between tumor and normal samples in the TCGA database, we discovered GLS expression was notably upregulated in various malignancies, including CHOL, COAD, ESCA, HNSC, LIHC, and STAD, whereas that was significantly downregulated in BRCA, GBM, KICH, KIRC, KIRP, LUAD, LUSC, PCPG, and UCEC (Fig. 2A). After matching TCGA samples with GTEx data, upregulated GLS were found additionally in DLBC, LAML, PAAD, READ, and THYM, but downregulated GLS were observed additionally in ACC, BLCA, CESC, LGG, OV, PRAD, SKCM, THCA, and UCS (Fig. 2B). Additionally, differential expression of paired samples between tumor tissues and adjacent tissues was observed in BRCA, CHOL, ESCA, HNSC, KICH, KIRC, LIHC, LUSC, PRAD, STAD, THCA, and UCEC (Fig. 2C). Overall, we were surprised to notice GLS was upregulated in the majority of digestive malignancies, while that was downregulated in almost all urogenital malignancies. Notably, we unveiled a significant positive co-expression relationship between GLS and currently known CRGs except the CDKN2A gene (Fig. 2D). In the HPA database, compared with normal tissues, higher IHC staining was observed in colon cancer, cutaneous melanoma, thyroid cancer, pancreatic carcinoid, lung cancer, and lymphoma (Fig. 2E). In terms of the total protein levels, the analysis results based on CPTAC samples uncovered the significantly upregulated protein expression of GLS in COAD, HNSC, and LIHC,

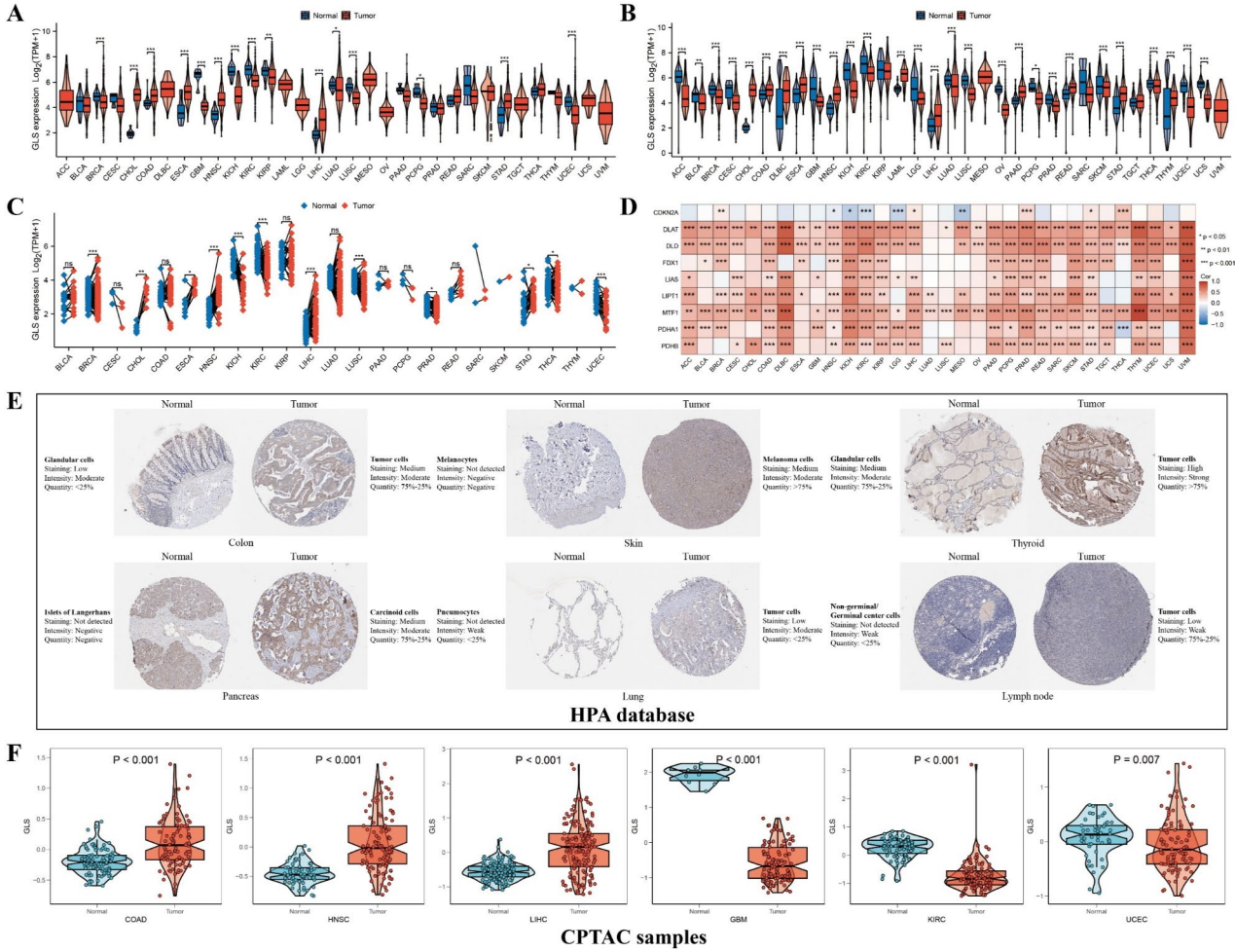

Fig. 2. Differential expression of GLS in pan-cancer. (**A**) GLS mRNA expression between tumor tissues and unpaired normal tissues in TCGA samples. (**B**) GLS mRNA expression between tumor tissues and unpaired normal tissues in the matched TCGA and GTEx samples. (**C**) GLS mRNA expression between tumor tissues and paired normal tissues in TCGA samples. (**D**) Co-expression relationship between GLS and other 9 cuproptosis-related genes in TCGA cancers. (**E**) GLS protein expression in tumor and normal tissues based on the immunohistochemical images of HPA database. (**F**) Total protein levels of GLS between tumor and normal tissues in CPTAC samples. $^{*}p < 0.05$; $^{**}p < 0.01$; $^{***}p < 0.001$.

but downregulated expression in GBM, KIRC, and UCEC (Fig. 2F). These differences were consistent with the trend of GLS mRNA expression in the corresponding tumors.

GLS expression is relevant to clinical characteristics in human cancers

With the assistance of the TNMplot tools, we attempted to explore the connection between GLS expression and tumor-metastatic progression. We noticed a trend toward higher GLS expression in metastatic tumor tissues compared with normal and primary tumor tissues in esophageal, hepatocellular, and skin cutaneous melanoma, as well as thyroid cancers (Fig. 3A). After that, we made a thorough inquiry about the expression differences of GLS in further detailed clinical characteristics. Interestingly, we realized GLS expression levels were upregulated in KIRC, KIRP, LIHC, and LUAD in women compared with that in men (Fig. 3B). We also found GLS expression levels in BRCA, KIRP, LIHC, and PAAD were increased in the patients aged 60 years or less compared with that in the older (Fig. 3C). Furthermore, we uncovered that GLS expression was associated with the pathological features in many cancers. Specifically, the differential expression of GLS was detected in KIRP, LIHC, PRAD, READ, and THCA based on the categories of T stage (Fig. 3D). Likewise, that was found in KIRP, LIHC, PRAD, and THCA based on the categories of N stage (Fig. 3E). Also, we indicated the significant connection between GLS expression and histological grades in LIHC and UCEC (Fig. 3F). Additionally, we clearly observed GLS expression was associated with TNM stages in KIRP, LIHC, THCA, and UCEC (Fig. 3G). Taken together, these findings indicated a strong association between GLS expression and advanced clinicopathology in multiple tumors, especially in LIHC, KIRP, and THCA.

GLS is a prognostic biomarker in human cancers

In TCGA and TARGET cohorts, we discovered high GLS expression was correlated with worse OS in STAD, BRCA, ESCA, HNSC, KIRP, LAML, LGG, LIHC, MESO, and UCEC, worse PFI in BLCA, CESC, COAD, LUSC, PRAD, SKCM-primary (SKCM-P), and UVM, and worse DFI in KIPAN (KICH, KIRC, and KIRP), PAAD, and THCA (Fig. 4). In the Kaplan-Meier Plotter database, we noticed that the patients with higher GLS expression in gastric, liver, colon, and ovarian cancer had significantly worse OS (**Fig. S1**). Collectively, high GLS expression was well established to predict poor prognosis in these 20 tumor types, including BLCA, BRCA, CESC, COAD, ESCA, HNSC, KIRP, LAML, LGG, LIHC, LUSC, MESO, OV, PAAD, PRAD, SKCM, STAD, THCA, UCEC and UVM.

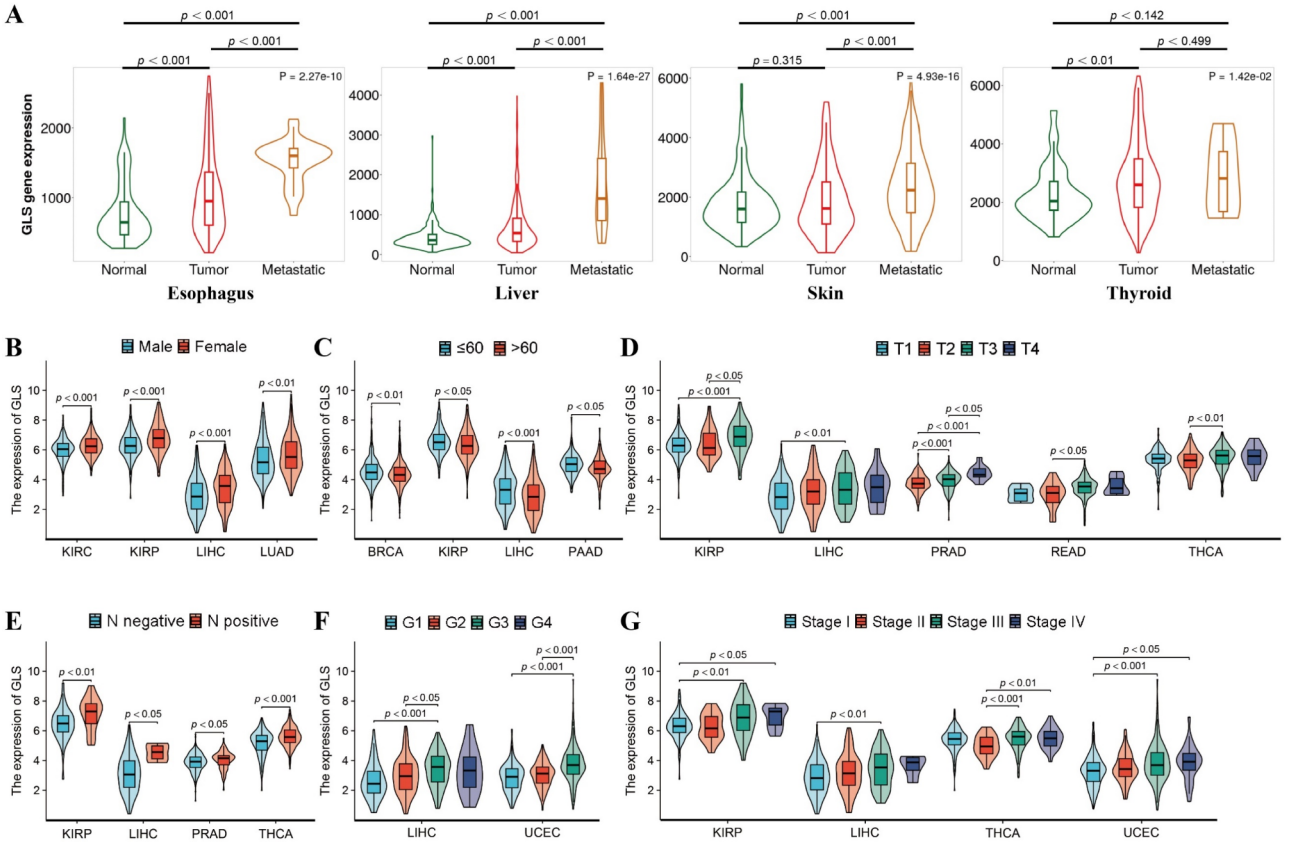

Fig. 3. Relationship between GLS expression and clinical characteristics in pan-cancer. (**A**) Association between GLS expression and tumor metastasis in TNMplot database. (**B**-**G**) Differential expression of GLS in different genders (**B**), ages (**C**), T stages (**D**), N stages (**E**), pathological grades (**F**), and TNM stages (**G**) based on TCGA data.

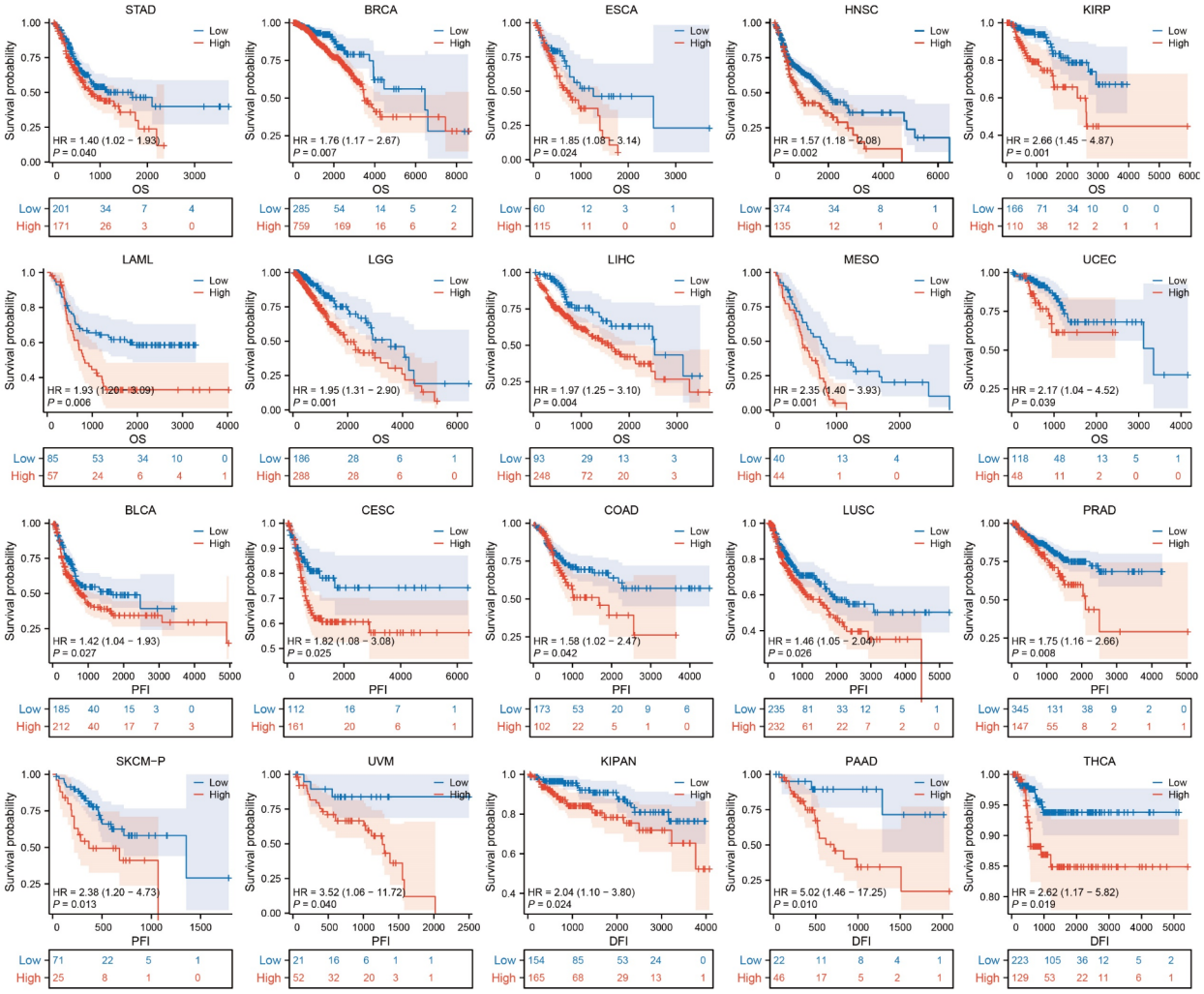

Fig. 4. Survival analysis of GLS expression in pan-cancer, including OS, PFI, and DFI.

Single-cell functional analysis and spatial transcriptomic atlas of GLS in human cancers

Single-cell sequencing analysis was conducted via the CancerSEA database to examine whether GLS was relevant to different functional states of tumor cells at single-cell resolution. As displayed in Fig. 5A, GLS expression was positively relevant to tumor stemness, epithelial-mesenchymal transition (EMT), and inflammation in multiple tumor types, but these correlations were relatively weak. Detailed relevance between GLS expression and 14 functional states across distinct cancers is displayed in **Table S5**. Then, we investigated the correlation between GLS and the functional states in specific single-cell tumor samples. The results indicated GLS expression levels were strongly positively relevant to metastasis, inflammation, EMT, and proliferation in AML, positively relevant to angiogenesis and inflammation in retinoblastoma (RB), and negatively relevant to DNA repair, DNA damage, and apoptosis in UVM (Fig. 5B). Meanwhile, the T-SNE diagrams showed GLS expression distribution at single-cell resolution in LAML, RB, and UVM.

Since the above findings didn't address the biological roles of GLS in STAD, single-cell analyses were performed specifically to elucidate that. As demonstrated in Fig. 5C, different cell populations in STAD were clearly distinguished in the UMAP diagram, and differential GLS expression among different cells was shown. We found GLS expression was relatively higher in malignant cells among different cell lineages (Fig. 5D). Meanwhile, we noticed the proportions of $CD8^+$ T lymphocytes, plasma cells, and fibroblasts were reduced by about half in the GLS-positive group compared with the GLS-negative group in STAD (Fig. 5E). Furthermore, some notorious cancer-related pathways were significantly enriched in STAD. The immunological pathways such as "IL6 JAK STAT3 Signaling" and "Inflammatory Response", the metabolic and mitochondrial pathways related to glutamine metabolism and oxidative phosphorylation, and the proliferation and cell death pathways such as "Myc Targets", "Cuproptosis" and "Apoptosis", as well as multiple key cancer-related signaling such as "PI3K Akt MTOR Signaling", "MTORC1 Signaling", "Hypoxia", "EMT" and "KRAS Signaling", were significantly observed in GLS-positive malignant cells (Fig. 5F). These findings imply GLS may have the potential to regulate

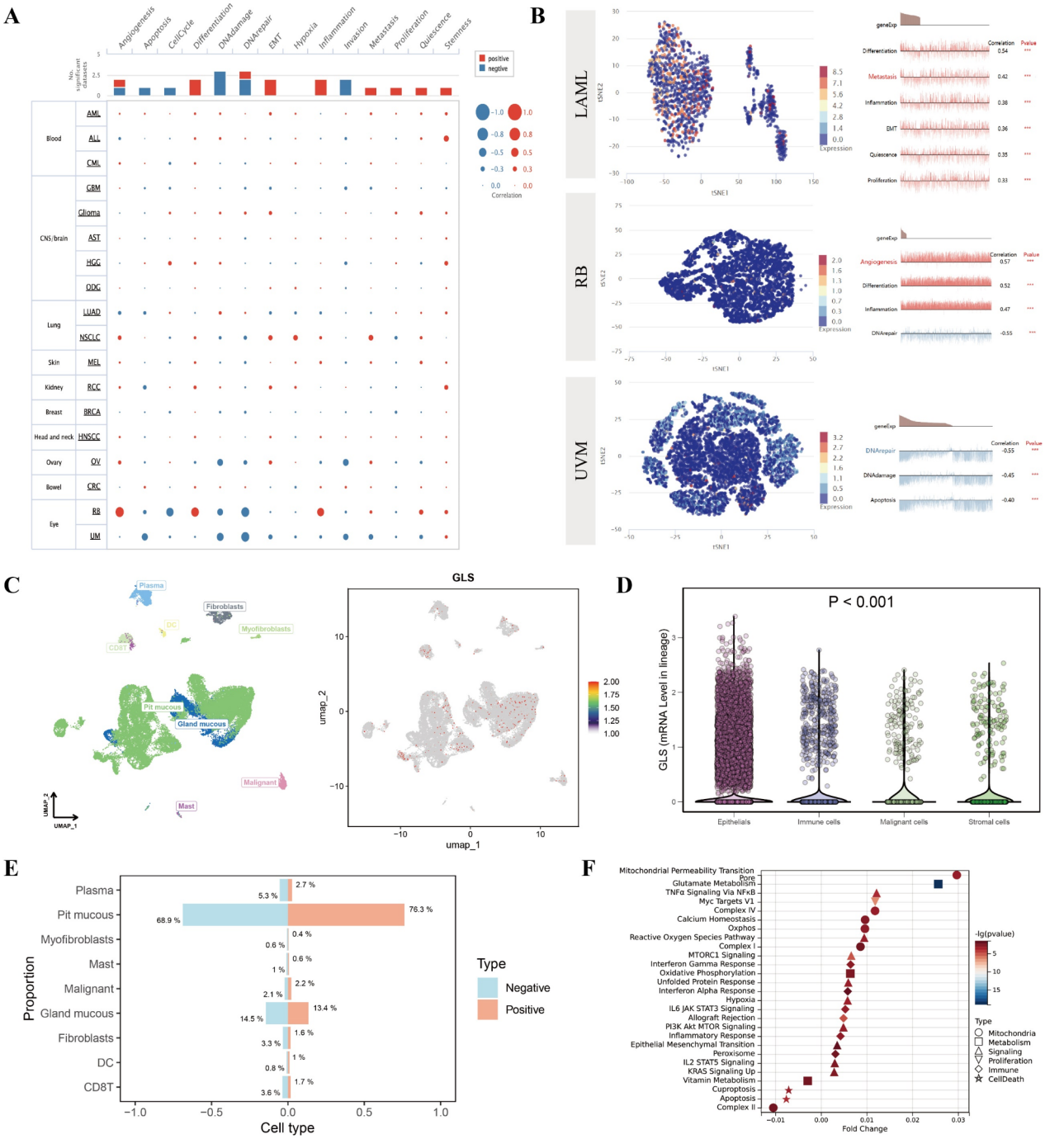

Fig. 5. Analysis of tumor single-cell sequencing in pan-cancer. (**A**) Correlation between GLS expression and 14 single-cell functional states. (**B**) T-SNE expression diagram and the most significantly correlated single-cell functional states in AML, RB, and UM samples. (**C**) Cell type annotation and GLS expression identification by UMAP in STAD. (**D**) Differential expression of GLS among different lineages in STAD. (**E**) Proportion of each cell type in GLS-positive and GLS-negative expression groups in STAD. (**F**) Biological pathways with significant differences between GLS-positive and GLS-negative groups in malignant cells of STAD. $^{***}p < 0.001$.

tumor immunity, metabolism, proliferation, progression, and cell death, which warrants further investigation and experimental validation.

Meanwhile, we elucidated the spatial expression patterns of GLS in human tumor samples based on single-cell transcriptomic and spatial transcriptomic data. As demonstrated in Fig. 6, we found GLS expression had a highly similar spatial localization to that of tumor cells in BRCA, colorectal cancer (CRC), KIRC, LUAD, LUSC, OV, SKCM, and gastrointestinal stromal tumors (GIST). In these tumor tissues, higher GLS expression levels

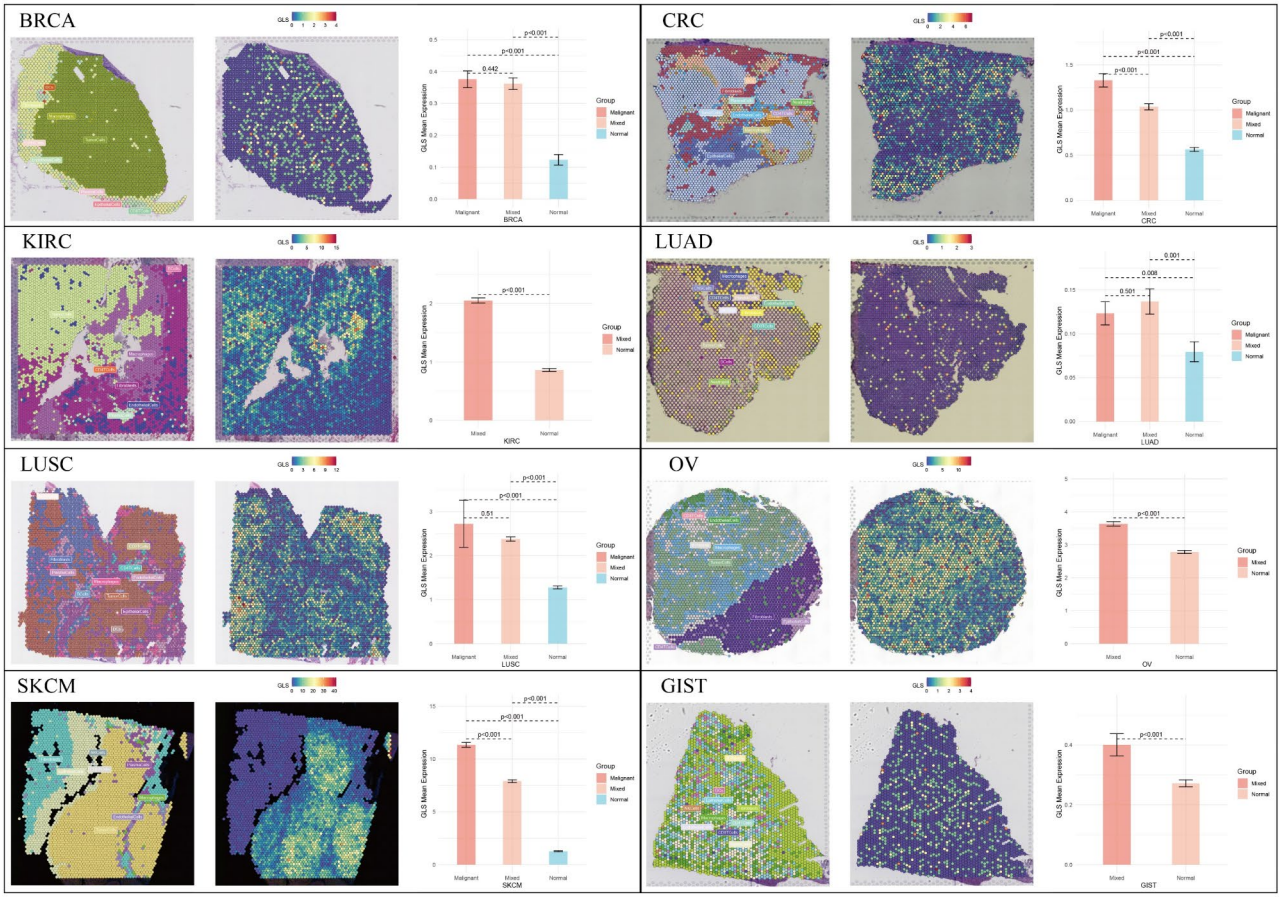

Fig. 6. Spatial transcriptome expression atlas of GLS in human cancers.

were observed in malignant and mixed-malignant spots compared to the spots composed of non-malignant cells, in which GLS expression levels were the lowest. These findings imply that the spatial expression of GLS in TME is mainly derived from tumor cells, and therefore tumor cells may have a stronger ability to utilize glutamine than non-tumor cells such as immune cells.

GLS expression is associated with genetic alteration and genomic heterogeneity

We queried the information on GLS alteration across TCGA pan-cancer cohorts through retrieving the cBioPortal database. As indicated in Fig. 7A, its alteration frequency in UCEC was the highest (5.86%), and mutation and amplification were the two dominating types in all TCGA tumors. As displayed in Figs. 7B and 103 mutation sites were identified in its protein structure where the genetic missense was the most common mutation type. The mutation sites seemed to be mainly concentrated in the glutaminase component segment (244–530). For example, we observed the occurrence of missense or nonsense mutations (amino acid change: R387Q) with underlying clinical significance in three UCEC patients. Their detailed mutation sites were shown in the stereoscopic protein structure of GLS (Fig. 7C). To further investigate the significance of GLS mutation for UCEC patients, we explored the association between GLS mutation and multiple infiltrated immune cells via the TIMER2.0 database. Obviously, the cohorts with mutated GLS in UCEC samples showed more abundances of $CD8^+$ T cells, B cells, myeloid dendritic cells, and M1 macrophages than the cohorts with wild-type GLS (**Fig. S2**). This could mean GLS mutation affects its enzymatic metabolic activity, resulting in changes in the immune cell infiltration and tumor immune microenvironment. Unfortunately, there is currently a lack of data to elucidate the roles of GLS mutations in UCEC prognosis.

Moreover, the relevance between GLS and genomic heterogeneity was analyzed. We witnessed GLS expression had a significant positive relevance to chromosome ploidy in COAD, STAD, and UCEC (Fig. 7D), suggesting that high-GLS expression may cause abnormal chromosome numbers in tumor cells. We also discovered GLS expression had a significant positive relevance to HRD in eight tumors, including BRCA, COAD, HNSC, KIRP, LIHC, PRAD, STAD, and UCEC, implying that the homologous recombination repair of these tumor cells is dysfunctional and patients with high-GLS expression may be highly sensitive to poly (ADP-ribose) polymerase (PARP) inhibitors and platinum-based chemotherapy agents (Fig. 7E). Simultaneously, we found higher GLS expression predicted higher MATH, that is, the greater tumor heterogeneity, in COAD, LIHC, LUAD, STAD, and UCEC (Fig. 7F). Overall, these results demonstrated GLS expression levels were dramatically relevant to

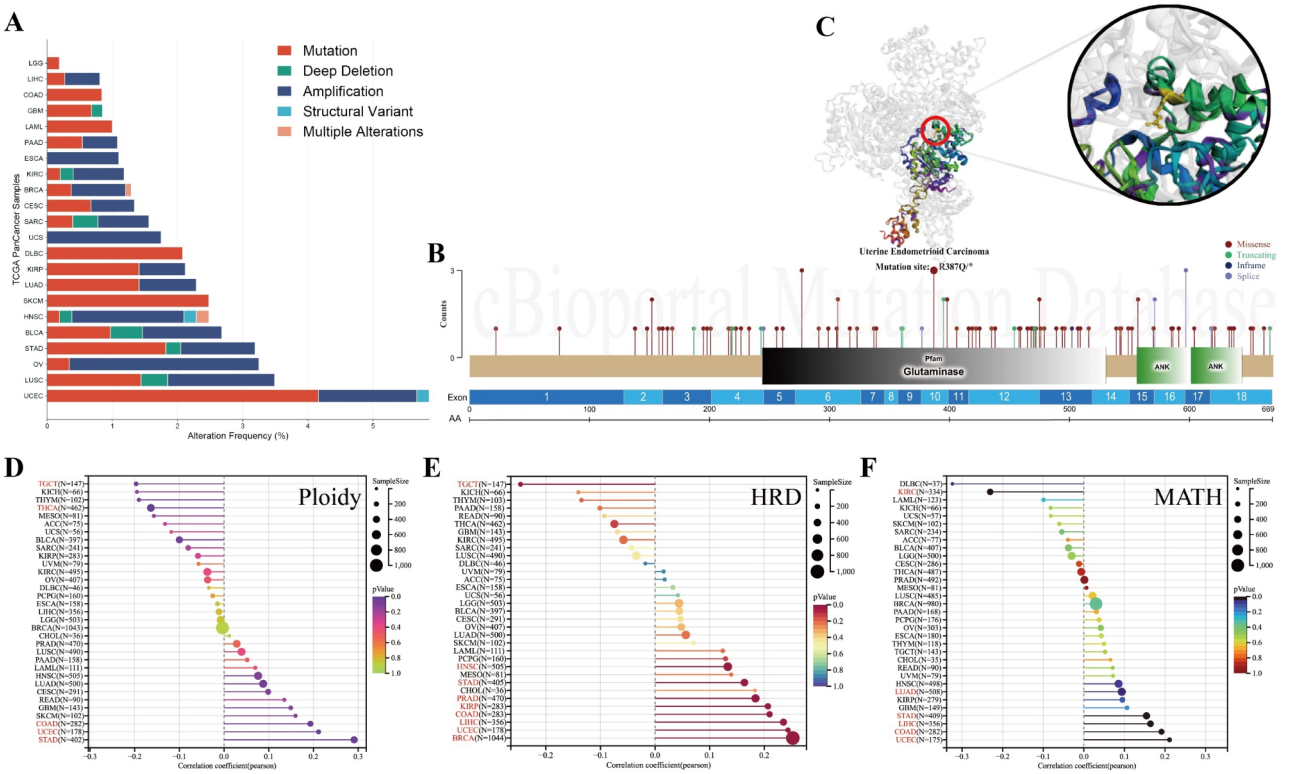

Fig. 7. Landscapes of genetic alteration and genomic heterogeneity in pan-cancer. (**A**) GLS alteration frequency across TCGA pan-cancer cohorts of cBioPortal database. (**B**) 103 mutation sites in the protein structure of GLS based on the cBioPortal database. (**C**) The stereoscopic protein structure of GLS and mutation site (AA change: R387Q) in UCEC. (**D-F**) Roles of GLS alteration in the genomic heterogeneity, including chromosome ploidy (**D**), HRD (**E**), and MATH (**F**).

increased genomic instability and tumor heterogeneity, especially in STAD, COAD, LIHC, and UCEC, which may be one of the reasons for their worse prognosis.

GLS expression is relevant to the therapeutic sensitivity of antitumor drugs

We analyzed whether GLS expression levels were relevant to the sensitivity of antitumor drugs utilizing the pharmacogenomic datasets in the CellMiner database where we selected the classical NCI-60 cancer cells to detect the activities of drugs in vitro. The findings indicated GLS expression was relevant to enhanced activities of various targeted drugs, such as afatinib, dacomitinib, erdafitinib, erlotinib, gefitinib, ibrutinib, lapatinib, midostaurin, neratinib, and vandetanib. However, GLS expression was associated with therapeutic resistance to several common chemotherapy and endocrine therapy drugs, such as actinomycin D, docetaxel, fulvestrant, vinorelbine, and paclitaxel (Fig. 8). These results provide substantial implications and references for the selection of clinical treatment strategies and individualized precision therapy.

GLS expression regulates various cell infiltration in the TME

We performed ssGSEA analysis on the above tumor types whose prognosis is associated with GLS, and the results demonstrated high GLS expression was significantly relevant to various immune cell infiltration in the TME. Specifically, in COAD, infiltrated B cells, T cells, Th17 cells, DCs, NK cells, and cytotoxic cells decreased in the high-GLS samples (Fig. 9A). In HNSC, infiltrated B cells, T cells, $CD8^+$ T cells, Th17 cells, DCs, and cytotoxic cells decreased in the high-GLS samples, while Th2 cell infiltration increased in that (Fig. 9B). In KIRP, the infiltration of $CD8^+$ T cells, DCs, eosinophils, NK cells, and cytotoxic cells decreased in the high-GLS subgroup, while Th2 cell infiltration increased in that (Fig. 9C). In LAML, the levels of Th17 cells, DCs, eosinophils, macrophages, and neutrophils decreased in the high-GLS subgroup, while mast cell infiltration increased in that (Fig. 9D). In LGG, high-GLS expression meant less infiltrated levels of $CD8^+$ T cells, Th17 cells, and DCs, whereas more infiltration of Th2 cells and mast cells (Fig. 9E). In LIHC, high-GLS expression meant less infiltration of Th17 cells, DCs, neutrophils, and cytotoxic cells, but more infiltration of Th2 cells (Fig. 9F). In STAD, high-GLS levels meant less infiltration of $CD8^+$ T cells, Th17 cells, DCs, and NK cells, while more infiltration of Th2 cells (Fig. 9G). In UCEC, high-GLS levels meant less infiltrated levels of B cells, T cells, Th17 cells, and cytotoxic cells, while also more infiltration of Th2 cells (Fig. 9H). Overall, high-GLS expression was relevant to the reduction of B cells, $CD8^+$ T cells, Th17 cells, DCs, NK cells, and cytotoxic cells, and the increase of Th2 cells in the TME.

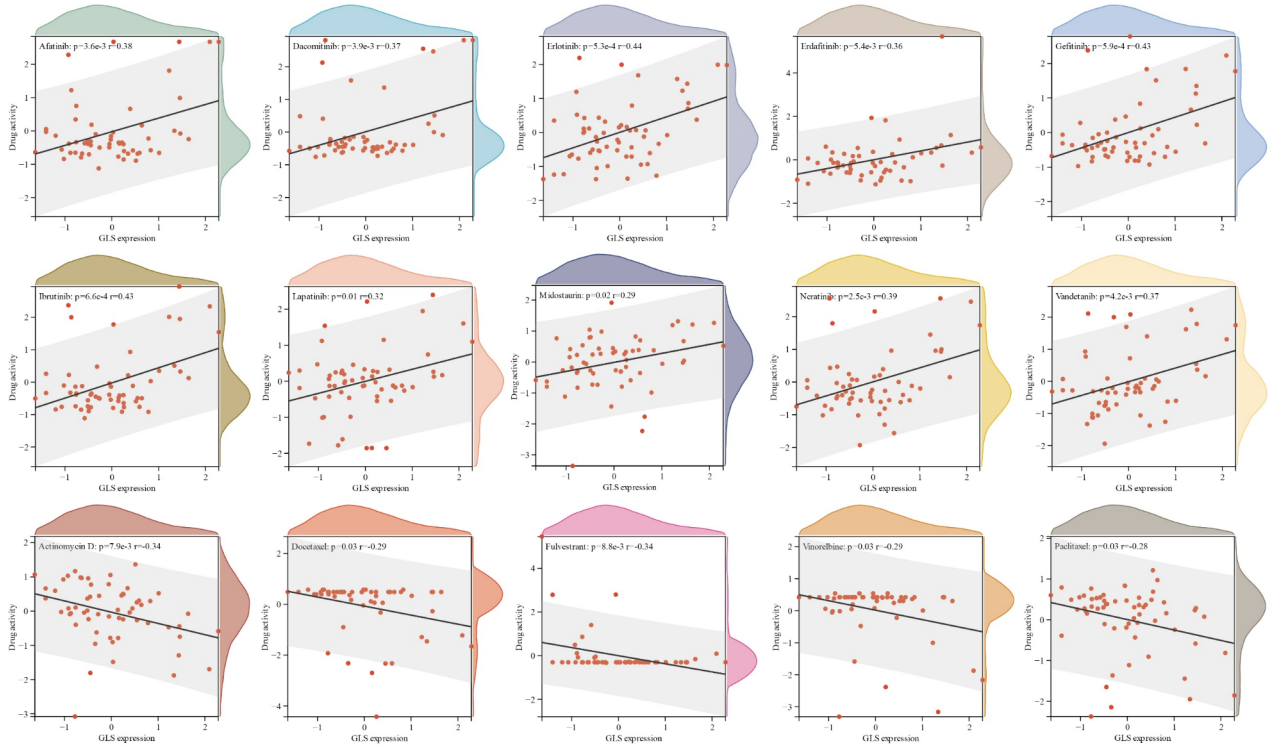

Fig. 8. Roles of GLS expression in antitumor drug activities, including afatinib, dacomitinib, erdafitinib, erlotinib, gefitinib, ibrutinib, lapatinib, midostaurin, neratinib, vandetanib, actinomycin D, docetaxel, fulvestrant, vinorelbine, and paclitaxel.

The findings from TIMER2.0 also revealed GLS expression was significantly negatively related to antineoplastic Th1 cell infiltration across almost all tumors, while it's positively relevant to cancer-promoting Th2 cell infiltration across most tumor types (Fig. 9I). Simultaneously, GLS expression was negatively correlated with anti-tumor $CD8^+$ T lymphocyte abundance in HNSC, UCEC, and CESC (Fig. 9J). Then, we were surprised to discover GLS expression levels were significantly positively associated with CAF infiltration across almost all tumors, such as BRCA, COAD, ESCA, HNSC, LIHC, LUSC, OV, PAAD, and UCEC (Fig. 9K). This provides crucial evidence that high-GLS levels are relevant to poor survival in these tumors. For endothelial cells, with the increase of GLS expression, we observed that the infiltrated abundances intensified significantly in six tumor types, including COAD, HNSC, LUSC, OV, PAAD, and TGCT (Fig. 9L), which may be relevant to the enhanced angiogenesis of these tumors with poor survival. In terms of immunosuppressive Tregs, there were higher infiltration levels with the increase of GLS expression in LIHC and THCA (Fig. 9M). Furthermore, as shown in Fig. 9N, the increased infiltration of immunosuppressive MDSCs was detected in multiple tumors with poor survival, such as COAD, HNSC, LGG, LIHC, and UCEC. Overall, GLS expression may be an immunological biomarker of the TME favorable to tumorigenesis and progression.

GLS expression is related to immunoregulation and immunotherapy

The relevance between the GLS expression and immunomodulatory genes was explored. As displayed in Fig. 10A, the expression of almost all 24 immunoinhibitory checkpoints was strongly positively associated with GLS expression in the overwhelming majority of tumor types. Of note, we witnessed the expression levels of CD274 (PD-L1) in 25 tumors, PDCD1 (PD-1) in 10 tumors, and CTLA4 in 16 tumors were significantly positively correlated with GLS expression (Fig. 10A), suggesting GLS expression might be associated with more immune brakes and immune escape in these tumors that covered almost all tumor types with poor prognosis associated with GLS expression. Additionally, a large number of chemokines were found to be positively related to GLS in the vast majority of TCGA tumors, especially in BRCA, HNSC, LIHC, LUSC, PAAD, THCA, UCEC, ACC, LUAD, PCPG, PRAD, and BLCA (Fig. 10B). Consistent with chemokines, the majority of chemokine receptors in these tumors were also positively associated with GLS expression (Fig. 10C). For instance, the expression levels of CCR1, CCR2, CCR3, CCR4, CCR5, CCR6, CCR8, CCR9, CXCR2, CXCR4, CXCR6 and CX3CR1 were positively associated with GLS expression in a host of tumors. These findings implied targeting GLS was likely to play non-negligible roles in the immunotherapy against chemokine receptors.

Since only small subsets of tumor patients can benefit from ICI immunotherapy, we further investigated its relationship with MSI, TMB, neoantigen, and IPS scores to predict immunotherapeutic response in tumor patients. Unfortunately, we noticed the patients who were detected high-GLS levels had lower MSI in COAD, HNSC, DLBC, KICH, and PRAD (Fig. 10D), fewer TMB in COAD, STAD, and CHOL (Fig. 10E), and fewer

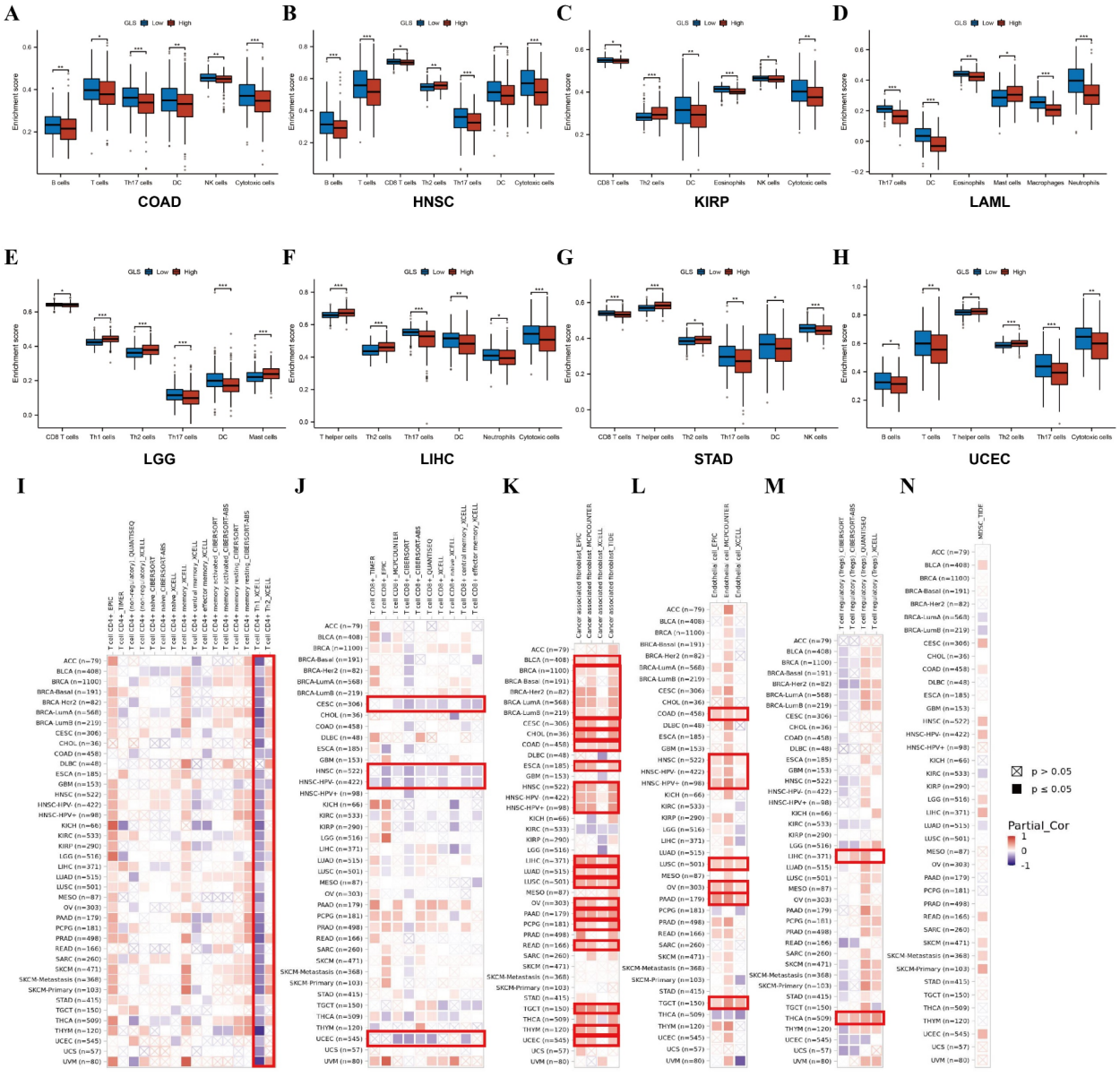

Fig. 9. Roles of GLS expression in TME in pan-cancer. (**A**-**H**) Differences of various immune cell infiltration between different GLS expression subgroups across TCGA pan-cancer cohorts. (**I**-**N**) Correlation between GLS expression and the infiltration of immune and stroma cells, including $CD4^+$ T cells (**I**), $CD8^+$ T cells (**J**), CAFs (**K**), ECs (**L**), Tregs (**M**), and MDSCs (**N**). $^*p < 0.05$; $^{**}p < 0.01$; $^{***}p < 0.001$.

neoantigens in COAD and CHOL (Fig. 10F), which meant GLS expression may be associated with weaker immunogenicity in these tumors. Meanwhile, the immunotherapeutic prediction analyses in different tumors revealed that IPS scores decreased to varying degrees in different subgroups with high-GLS expression. Predictably, for the patients with high GLS levels in COAD, the combined application of CTLA4 and PD-1/PD-L1 inhibitors might have a worse immunotherapeutic response (Fig. 10G). Worse yet, for the patients with high-GLS expression in STAD, UCEC, SKCM, and OV, multiple immunotherapeutic modalities, including anti-CTLA4, anti-PD-1/anti-PD-L1, and combination treatment, might have poorer clinical efficacy (Fig. 10H). Additionally, high-GLS expression predicted a worse response to anti-PD-1/anti-PD-L1 treatment in BRCA, KIRP, LIHC, and THCA (Fig. 10I).

We further explored the predictive roles of GLS utilizing two independent immunotherapy cohorts, including the metastatic urothelial carcinoma (IMvigor210) cohort and the melanoma (GSE91061) cohort. As presented in Fig. 10J, we found GLS expression in the response subgroup was considerably lower than that in the non-response subgroup in the metastatic urothelial carcinoma with anti-PD-L1 treatment. Consistent with the response to immunotherapy, a lower expression level of GLS had a better clinical OS (Fig. 10L). In another melanoma cohort with anti-PD-1/anti-CTLA4 treatment, it was visible that the patients who responded to immunotherapy had a

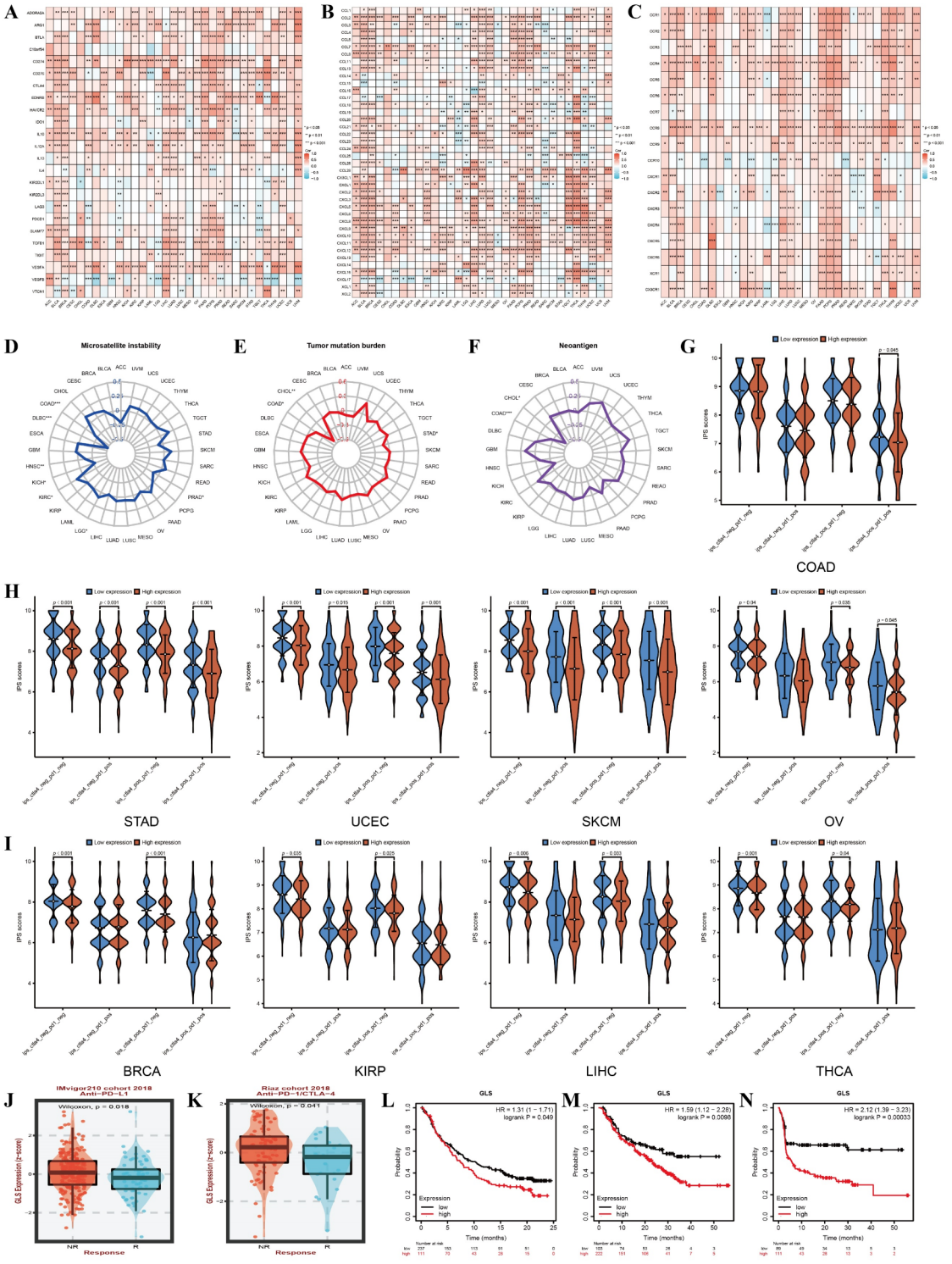

Fig. 10. Association of GLS expression with immunomodulatory genes and immunotherapy in pan-cancer. (**A**-**C**) Correlation heatmap between GLS expression and inhibitory immune checkpoints (**A**), chemokines (**B**), and chemokine receptors (**C**). (**D**-**F**) Relationship between GLS expression and MSI (**D**), TMB (**E**), and neoantigen (**F**). (**G**-**I**) Differences of IPS scores between different GLS expression subgroups in TCGA cohorts. (**J**, **K**) Expression levels of GLS in the patients with response and non-response to immunotherapy in the independent metastatic urothelial carcinoma cohort (**J**) and melanoma cohort (**K**). (**L**) Kaplan-Meier curves on OS for patients with high and low GLS expression in urothelial carcinoma. (**M**, **N**) Kaplan-Meier curves on OS (**M**) and PFS (**N**) for patients with high and low GLS expression in melanoma. $^{*}p < 0.05$; $^{**}p < 0.01$; $^{***}p < 0.001$.

dramatically lower expression level of GLS (Fig. 10K). The K-M curves supported lower expression level of GLS had a better clinical OS and progression-free survival (PFS) in melanoma (Fig. 10M, N). Taken together, patients with high expression levels of GLS may benefit less from immunotherapy for these abovementioned tumors, even though their PD-1/PD-L1/CTLA4 may be positive. Hence, immunotherapy in combination with targeting GLS as a logjam breaker may be a potential strategy to increase tumor immunogenicity and immunotherapy efficacy.

GLS-related genes and gene enrichment analysis in human cancers

The latent function and biomolecular mechanism of GLS in tumorigenesis and progression were investigated through gene enrichment analysis. Firstly, we established the PPI network based on the STRING database, where a total of 20 GLS-related interactors were obtained for subsequent analysis (**Fig. S3A**). Meanwhile, the top 100 similar genes were acquired via the GEPIA2 platform. We found GLS expression was strongly positively associated with GLS-related genes across almost all tumor types (**Fig. S3B**, **C**). Next, we integrated these 120 genes for KEGG and GO enrichment analysis (**Table S6**). The KEGG pathway analysis illustrated multiple metabolic pathways, such as "alanine, aspartate, and glutamate metabolism", "arginine biosynthesis", "glycine, serine, and threonine metabolism", "taurine and hypotaurine metabolism", "nitrogen metabolism", "carbon metabolism", "one carbon pool by folate", and "glyoxylate and dicarboxylate metabolism", were significantly enriched (Fig. 11A). The reprogramming of these metabolic pathways might act a pivotal part in tumorigenesis and progression. The GO analysis also illustrated that GLS-related genes were significantly associated with the amino acid metabolism process and molecular transmembrane transport (Fig. 11B). Detailed results about KEGG and GO enrichment analysis are provided in **Table S7**. The connection networks between the key GLS-related molecules and KEGG pathways and GO terms were exhibited in Fig. 11C.

To further seek the potential oncogenic pathways of GLS, the GSEA analyses were performed based on the GLS-classified differential genes, and the top five representative enrichment pathways were visualized across 20 tumor types with poor prognosis associated with GLS expression. The differential genes in each of the 20 cancers are shown in **Table S8**. As exhibited in Fig. 12, compared with the low GLS expression groups, common downregulated enrichment pathways in the high GLS expression groups included "innate immune system", "Fcγ receptor (FcγR) dependent phagocytosis", "FcγR activation", "antigen activates B cell receptor (BCR) leading to generation of second messengers", "CD22 mediated BCR regulation", "signaling by the BCR", and "binding and uptake of ligands by scavenger receptors". Meanwhile, representative upregulated pathways in the high GLS expression groups included "extracellular matrix (ECM) organization", "degradation of the ECM", "ECM regulators", "ECM receptor interaction", and "collagen formation". These results fully confirm GLS expression is closely relevant to the decline of innate and adaptive immune responses and the increase of ECM remodeling and tumor migration in the immune microenvironment. Notably, we witnessed prominent enrichment of several classical carcinogenic signaling pathways at high GLS expression, such as PI3K/Akt/mTOR signaling axis and receptor tyrosine kinases signaling pathway in LIHC, and VEGFA/VEGFR2 signaling pathway and MAPK family signaling cascades in THCA. These aforementioned potential cancer-related pathways are conducive to understanding the molecular mechanism of GLS and developing targeted therapies and immunotherapies.

Validation analysis in GC population

Since we identified differential GLS expression as a potential biomarker of tumor progression and prognosis through public database analyses, it's essential to validate relevant findings using an actual clinical GC cohort. As demonstrated in Fig. 13A, GLS protein was mainly undetectable or had relatively weak staining detected in para-cancerous tissues, but relatively strong staining in tumor tissues. The GLS levels were higher in tumor tissues compared to para-tumor tissues based on the differential analyses in both matched and unmatched samples (Fig. 13B, C). Survival analysis revealed patients with low-GLS protein expression had a better OS (Fig. 13D). In the subgroup with high-GLS expression, GC patients had worse clinicopathological T stage (Fig. 13E) and N stage (Fig. 13F), as well as more lympho-vascular invasion (Fig. 13G). Univariate and multivariate Cox regression analyses revealed GLS protein levels were an independent risk factor for GC prognosis (Fig. 13H, I). These findings confirmed that high-GLS expression is an effective biomarker for GC progression and prognosis. Based on the excellent performance of GLS in GC prognosis, we constructed a nomogram using GLS H-score and clinical and pathological variables to forecast the prognosis of GC patients (Fig. 13J). The 3-, 5-, and 7-year AUC values were 0.681, 0.744, and 0.785, respectively, close to or greater than 0.70 (Fig. 13K). The 3-, 5-, and 7-year calibration curves confirmed that nomogram-based survival prediction matched well with the best predictive performance (Fig. 13L). However, in the nomogram constructed using clinical and pathological variables and without GLS H-score, the 3-, 5-, and 7-year AUC values were 0.631, 0.693, and 0.706, respectively, which was obviously worse in predictive performance than the nomogram constructed based on GLS expression (**Fig. S4**). In addition, the GLS-based risk scores had the greatest AUC values at 3, 5, and 7 years, compared to other clinical and pathological variables (Fig. 13M-O). These results explain the importance of GLS in the construction of nomogram model.

Validation analysis in GC cells in vitro

In addition to clinical cohort validation, the biological functions of GLS in GC cells remain to be elucidated. To further validate its carcinogenicity, we investigated its expression levels in GC cells in vitro and its regulatory roles in the proliferation, migration, invasion, and apoptosis of GC cells. GLS expression levels were relatively higher in MKN-1, AGS, and SNU-638 cells compared to normal GES-1 cells (Fig. 14A, C). Subsequently, we successfully inhibited the expression levels of GLS in AGS and SNU-638 GC cells by siGLS transfection (Fig. 14B, D). The CCK-8 assays demonstrated the suppression of GLS expression in GC cells could observably impede the proliferation of tumor cells at 48 h and 72 h after transfection (Fig. 14E, F). The wound-healing assays suggested

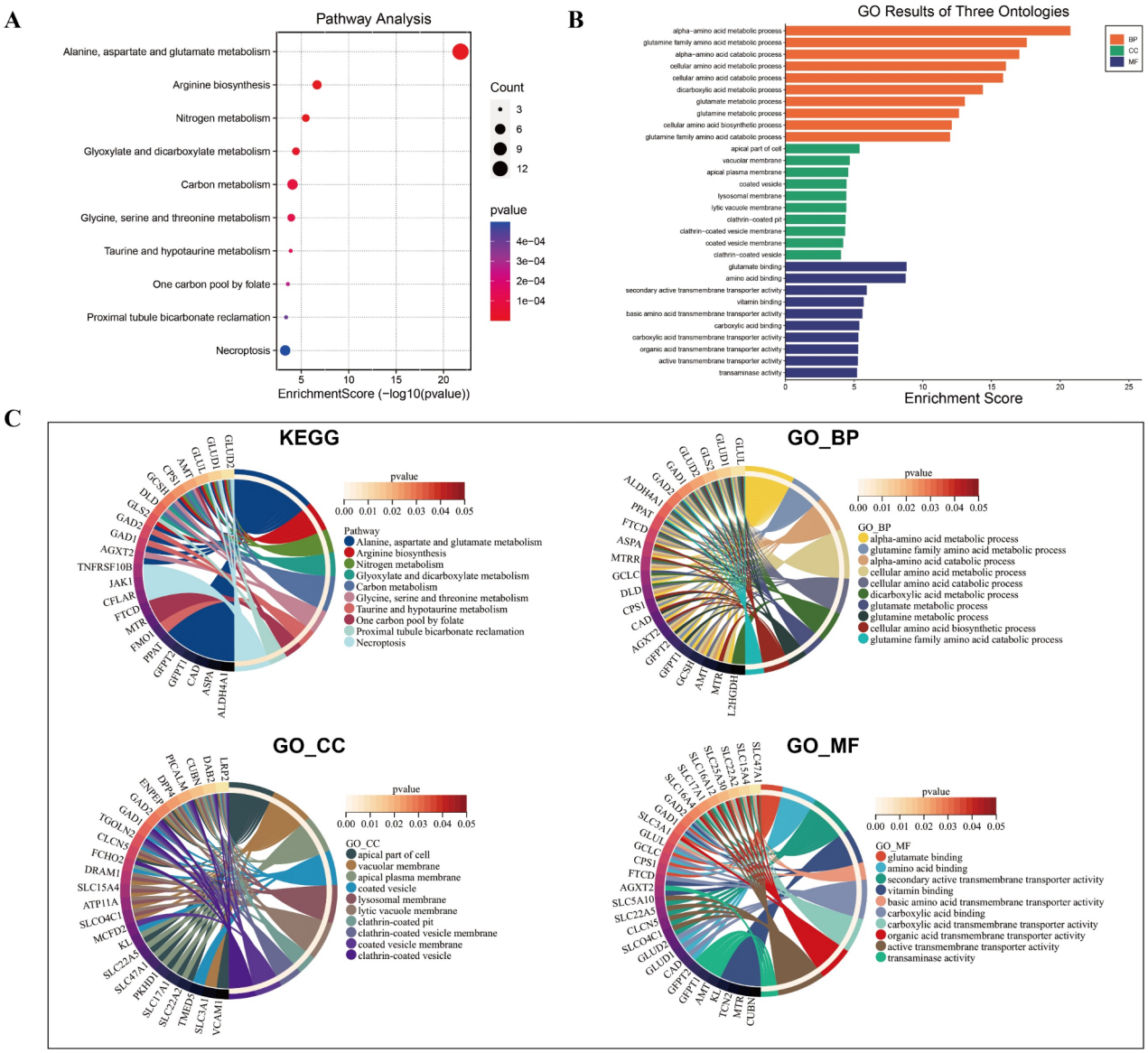

Fig. 11. KEGG and GO enrichment analysis. (**A**) KEGG pathway enrichment analysis. (**B**) GO functional enrichment analysis, including biological process (BP), cellular component (CC), and molecular function (MF). (**C**) Interactions of key GLS-related genes with KEGG pathway and GO terms.

that GLS downregulation in GC cells could significantly interfere with their migration ability (Fig. 14G, H). The transwell migration assays further confirmed that inhibiting GLS expression prominently reduced the number of GC cell migrations (Fig. 14I, J). Furthermore, we noticed the expressed downregulation of GLS could effectively attenuate the invasion ability of GC cells (Fig. 14K, L). Moreover, an increased percentage of apoptosis in GC cells was detected when GLS expression levels were suppressed (Fig. 14M, N). Together, these results imply that GLS plays a pivotal part in the oncological behavior including proliferation, migration, invasion, and apoptosis in GC.

Discussion

GLS, a gatekeeper of glutamine metabolism, reprograms the cellular energy metabolism and resists cellular oxidative stress, thus promoting tumorigenesis and progression[6,10,27]. Nevertheless, its underlying biological roles in tumor progression, prognosis, immune microenvironment, and immunotherapy remain unclarified. In this study, we conducted a pan-cancer analysis and related validation to understand its biological functions and oncogenic mechanisms. We noticed the expression levels of GLS mainly increased in digestive malignancies. These tumors may initiate the metabolic reprogramming of glutamine by upregulating GLS expression to sustain required energy metabolism, redox homeostasis, and biological synthesis. Nevertheless, the expression levels of GLS mainly decreased in urogenital malignancies. The reason we speculate is that the α-ketoglutarate,

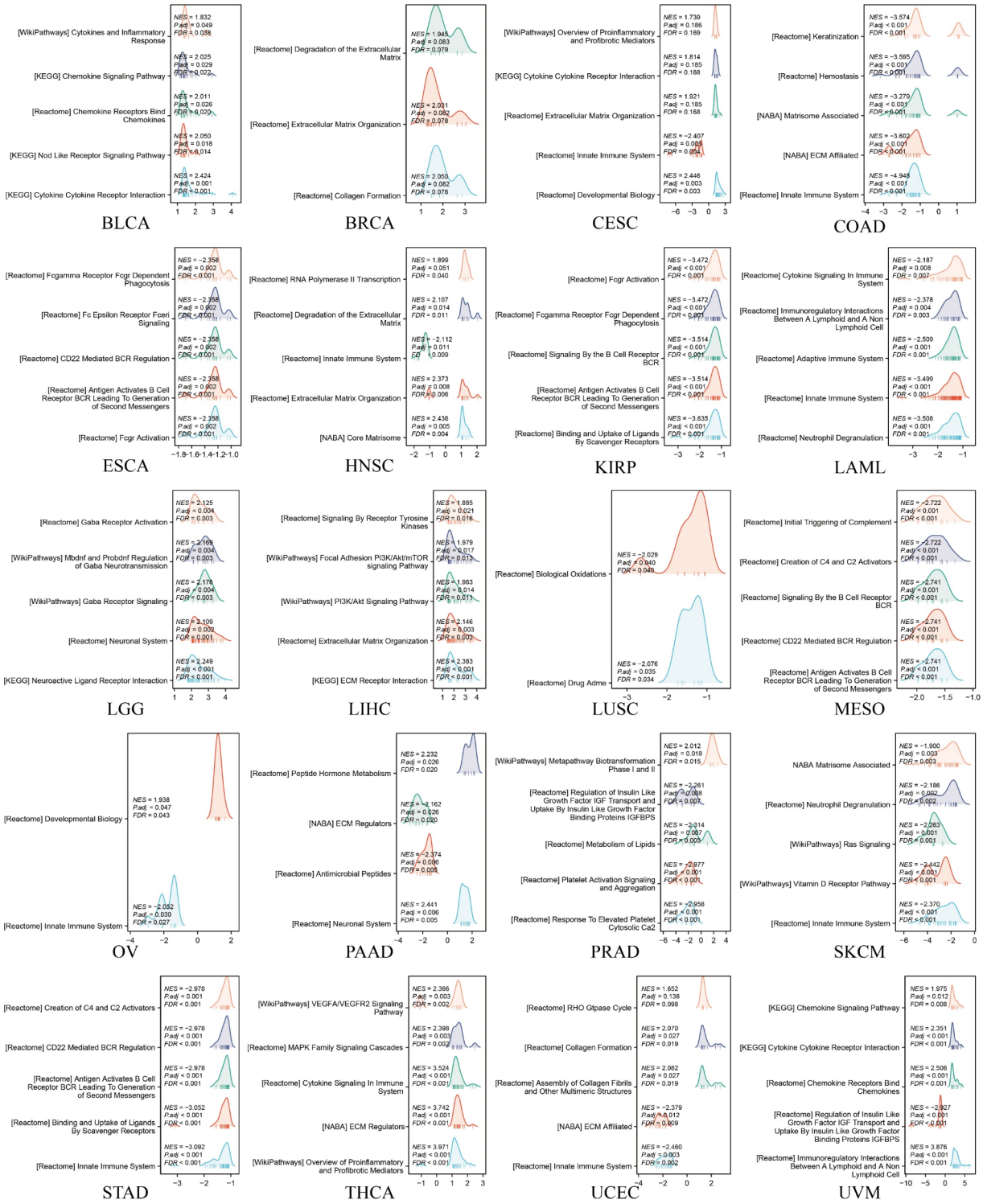

Fig. 12. GSEA enrichment analysis across the TCGA tumor cohorts.

a precursor required for the TCA cycle, may be supplemented primarily by gluconic glycolysis and pyruvate carboxylation rather than glutaminolysis in these cancers[14]. These findings suggest GLS may play heterogeneous roles in different tumor types, and the features of glutamine metabolism may depend on the origin of tumor tissues. Interestingly, we noticed GLS was more highly expressed in women and younger patients across multiple cancer types. We consider that GLS expression may be relevant to female estrogen levels, as previous research has confirmed that estrogen observably promotes GLS upregulation via c-Myc and enhances glutamine metabolism[28].

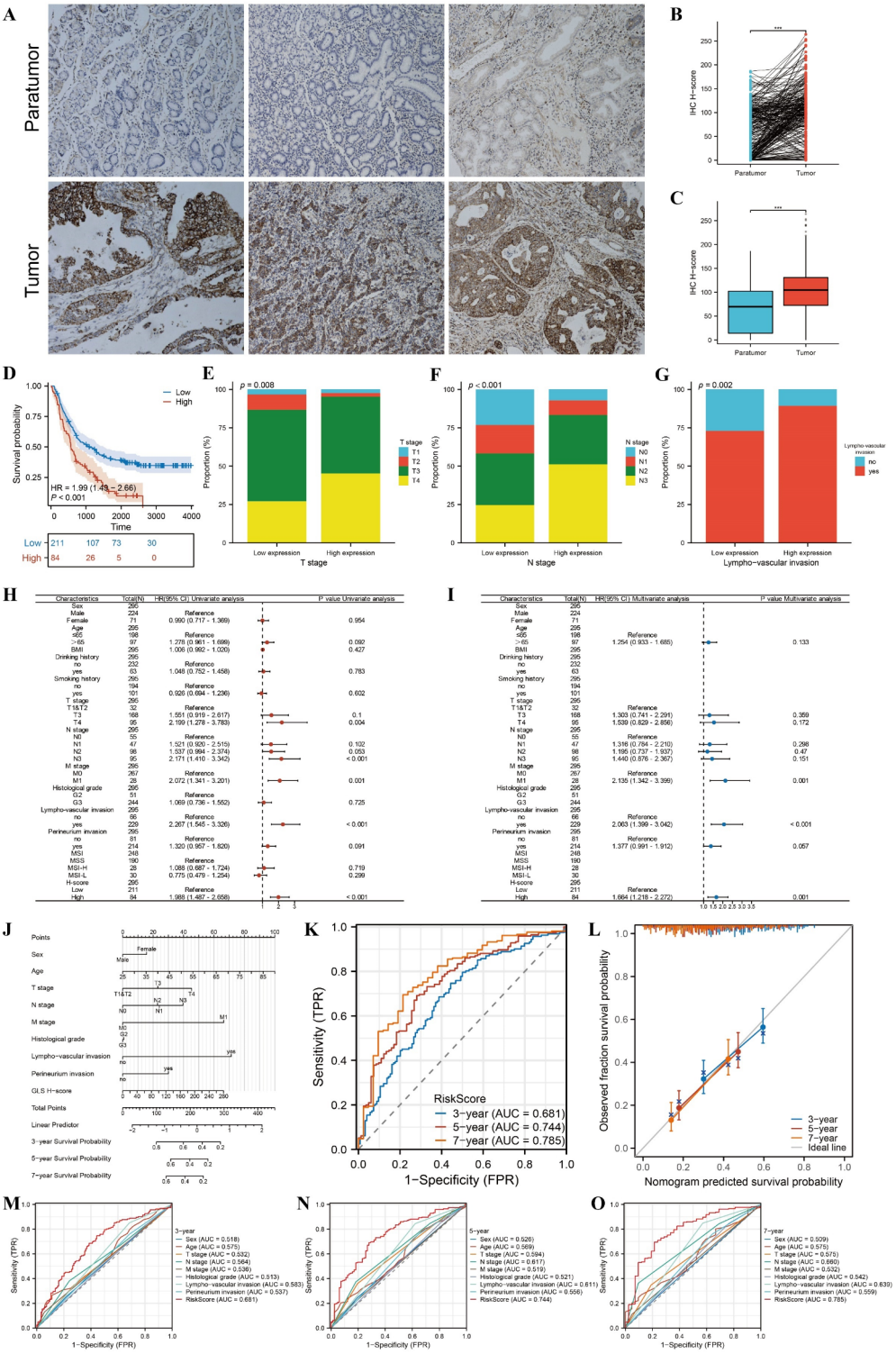

Fig. 13. Validation analysis in clinical GC cohort. (**A**) Representative GLS IHC images of tumor tissues and corresponding para-tumor tissues. (**B**) Differential expression of GLS protein between tumor tissues and paired normal tissues. (**C**) Differential expression of GLS protein between tumor tissues and unpaired normal tissues. (**D**) Differences in Kaplan-Meier curves for OS between different GLS expression subgroups. (**E-G**) Relationship between GLS expression and pathological T stage (**E**), N stage (**F**), and lympho-vascular invasion (**G**). (**H**, **I**) Univariate Cox regression analysis (**H**) and multivariate Cox regression analysis (**I**). (**J**) Nomogram for the prediction of 3-, 5- and 7-year OS in GC patients. (**K**) Time-dependent ROC curves of the nomogram. (**L**) Calibration curves of the nomogram. (**M-O**) Comparison of ROC curves of GLS-based risk scores and clinical and pathological variables at 3 (**M**), 5 (**N**), and 7 years (**O**). ***$p < 0.001$.

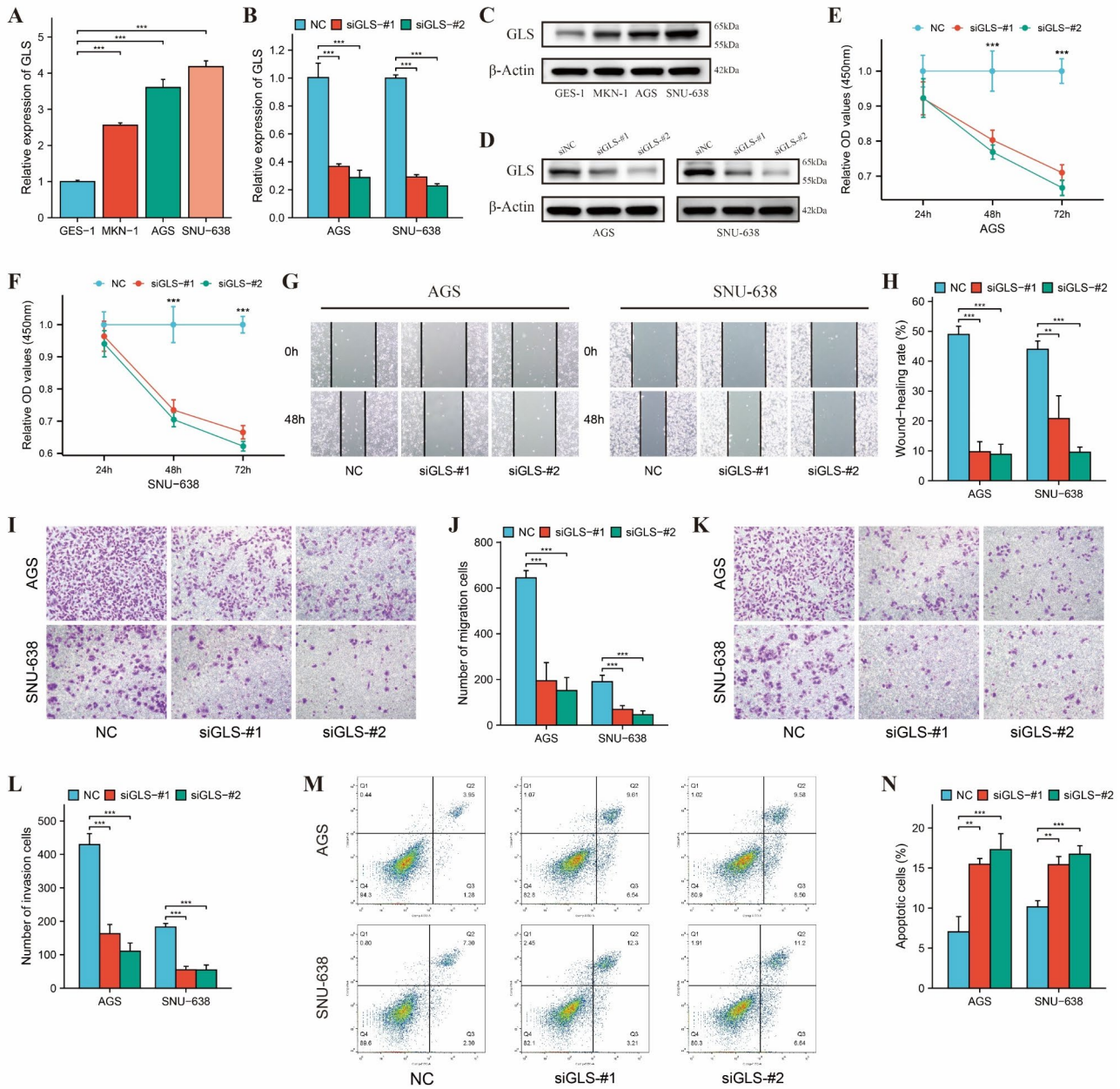

Fig. 14. Validation analysis in GC cells in vitro. (**A**) GLS mRNA expression in GC cells and normal gastric epithelial cells. (**B**) GLS mRNA expression in GC cells were inhibited by GLS-targeting siRNA. (**C**) GLS protein expression in GC cells and normal gastric epithelial cells. (**D**) GLS protein expression in GC cells were inhibited by GLS-targeting siRNA. (**E**, **F**) CCK-8 assays revealed that inhibition of GLS expression can significantly reduce the proliferation ability of AGS cells (**E**) and SNU-638 cells (**F**). (**G**, **H**) Wound healing assays revealed that inhibition of GLS expression can significantly reduce the migration distance of GC cells. (**I**, **J**) Transwell migration assays revealed that inhibition of GLS expression can significantly reduce the migration ability of GC cells. (**K**, **L**) Matrigel invasion assays revealed that inhibition of GLS expression can significantly reduce the invasion ability of GC cells. (**M**, **N**) Cell apoptosis assays revealed that inhibition of GLS expression can significantly induce the death of GC cells. $^{**}p < 0.01$; $^{***}p < 0.001$.

Our study found GLS expression was a considerable underlying biomarker for tumor progression and prognosis. For instance, in liver and stomach cancer, we noticed a strong relationship between GLS expression and advanced clinicopathologic characteristics and unfavorable survival outcomes. In vitro experiments also found that when GLS expression was suppressed, the proliferative activity and progress capacity of GC cells were dramatically reduced. These results were supported by previous research in liver and stomach tumors[29–31]. Notably, we witnessed GLS expression was observably relevant to different single-cell functional states of certain tumor cells, such as angiogenesis, EMT, and stemness. Evidence revealed that the vascular sprouting and pathological angiogenesis depended on the multiple essential metabolic pathways in endothelial cells, including

glutamine[32]. The scientific research demonstrated GLS inhibition reduced the endothelial sprouting and pathological angiogenesis, but supplementing the TCA cycle substrate could resume endothelial proliferation in the glutamine-deficient cells[33]. Furthermore, glutamine metabolism played a regulatory role in EMT, which was noticed in previous investigations in which GLS knockdown or glutamine deprivation upregulated E-cadherin and downregulated vimentin[34]. Moreover, evidence deciphered that glutaminolysis could induce tumor stemness properties and targeting GLS attenuated tumorous stemness by inhibiting the Wnt/β-catenin pathway[29,35]. Overall, these results suggest that GLS-mediated glutamine metabolic reprogramming is critical for assessing tumor progress and malignant hallmarks. Blocking this reprogramming is a potential antitumor therapeutic strategy that may ameliorate patients' outcomes.

The TME provides a sanctuary for tumor cells from immune destruction, where the tumor cells receive nutritional support for survival and metabolism. Abundant evidence suggested the TME influenced the therapeutic response and clinical prognosis, so targeting the TME components provided an opportunity for tumor therapy[36,37]. The metabolic reprogramming of tumors can shape the TME, thereby limiting immune response and providing an obstacle to oncotherapy[38]. We witnessed a significant decrease in multiple antitumor immune cells in the high-GLS expression subgroup, and even an increase in immunosuppressor cells and dysregulation of Th1/Th2 homeostasis in the TME, suggesting that the metabolic reprogramming of glutamine may disrupt antitumor immunity and assist tumor cells to achieve immune escape. Since both tumor proliferation and immune activation are highly dependent on glutamine, tumor cells and immune cells in the TME are constantly in a tug of war to compete for limited glutamine resources[39]. Spatial transcriptome analyses revealed the spatial expression of GLS in the TME was mainly derived from tumor cells, rather than non-tumor components such as immune cells. Hence, tumor cells with high-GLS involvement may gain priority over immune cells in the competition for acquisition and utilization of glutamine, which poses a severe challenge to immune cells to maintain their antitumor response and function[7]. Meanwhile, a host of immunosuppressive cells could take advantage of the opportunity to further deteriorate the antitumor immunity. Ample direct evidence demonstrated the influence of glutamine metabolism on $CD8^+$ T lymphocytes and the inhibition of corresponding glutamine metabolism could reestablish the TME favorable to the proliferation and activation of $CD8^+$T cells, thus making them present the characteristics of immune memory and enhance cytotoxicity[40–42]. Recent preclinical research also confirmed GLS inhibitor CB-839 can effectively improve the cytotoxicity of tumor-infiltrating lymphocytes against patient-derived melanoma cells[43]. Therefore, targeting GLS-mediated tumor metabolic reprogramming holds promise for reversing the vulnerable position of immune cells in glutamine competition and could provide valuable insights into precise TME regulation and innovative therapeutic strategies in future clinical practice.

Immunotherapy is one of the frontiers for human cancers. Despite some breakthroughs in immunotherapy, the overall therapeutic effect at the current stage remains unsatisfactory[44]. Since most patients cannot benefit from immunotherapy, it is urgent to evaluate which patients may be suitable for immunotherapy. In this research, we revealed that GLS expression levels were positively correlated with immunosuppressive checkpoints across almost all cancers, which provides the premise for the combination treatment program. Unfortunately, we found that patients with high GLS expression may not benefit from existing immunotherapies due to poor therapeutic response and survival, which may be attributed to cytotoxic lymphocytes failing in this battle to capture glutamine and thus losing their immunological effects[45]. Even worse, GLS-mediated glutamine metabolic reprogramming may be closely related to the cold tumor immune microenvironment, as it has been proven, after all, that inhibiting glutamine metabolism is conducive to the immunological transition from "cold" TME into "hot" TME[46,47]. Though this malignant metabolic hallmark is like a fog shrouding immunotherapy, once a breakthrough is made, it will become a new shine to remove obstacles for immunotherapy[48]. Given that, forward-looking researchers have now likened the regulation of glutamine metabolism to the rising star of antitumor immunotherapy[39]. Related preclinical studies revealed the combination of GLS antagonists and ICIs boosted the immunological infiltration and the function of T cells and improved the antitumor efficacy of ICIs in tumor-bearing mice[40,43,49]. Meanwhile, GLS inhibition has also achieved remarkable efficacy in adoptive cellular immunotherapy, such as CAR-T therapy[43,50]. Most notably, although the current scientific community generally recognizes that glutamine has a vital role in the proliferation and antitumor activity of immune cells, GLS inhibition didn't cause these cells to lose metabolic capacity, and instead, an enhancement in the number and function of lymphocytes were observed[40,50]. These breakthrough results have ignited an intense interest in the intricate crosstalk between GLS-mediated metabolic reprogramming and the TME. However, there is still an urgent need to conduct clinical trials to further confirm the efficacy and safety of targeted GLS combined immunotherapy in the future.

In addition to focusing on immunotherapy response, we also witnessed GLS expression was relevant to enhanced activities of various targeted drugs, but with therapeutic resistance of several common chemotherapy and endocrine therapy drugs. Recent investigations have recognized tumor metabolic reprogramming is closely relevant to antitumor drug sensitivity[51]. Overwhelming evidence has demonstrated glutamine reprogramming contributes to multidrug resistance of tumor cells, and targeting glutamine metabolism is an effective strategy to reverse therapeutic resistance[52,53]. A related mechanism may be that GLS inhibition is conducive to the consumption of glutathione that maintains redox homeostasis in tumor cells, thereby enhancing drug-induced oxidative damage[54]. Previous investigators confirmed the idea that GLS inhibitor could resume the radiosensitivity of non-small cell lung cancer patients undergoing radiotherapy by disrupting the redox balance[55]. These results not only strongly supported the influence of GLS-mediated glutamine metabolism on antitumor therapy, but provided substantial references for the selection of clinical treatment strategies and individualized combined precision therapy. Nevertheless, before translating these findings into clinical practice in the future, we still need to verify the exact effects of GLS expression on the activity of these drugs through in vivo and in vitro experiments.

Gene enrichment analysis not only further suggested that GLS expression might impair innate and adaptive immune responses, but also found multiple highly enriched tumorigenic pathways in certain cancers. For example, the PI3K/Akt/mTOR signaling pathway was significantly upregulated in LIHC. Evidence demonstrated GLS regulated cyclin D2 through enhancing the PI3K/Akt/mTOR signaling to promote cell proliferation and progress[56]. Interestingly, suppressing the mTOR pathway could also inhibit GLS activity, resulting in reduced glutamine-mediated tumor proliferation[57]. These findings imply that the interweaving between GLS and mTOR signaling should be bidirectional and the crosstalk between them may be progressively amplified like a rolling snowball. Notably, the inflammatory immune microenvironment involved in the pathogenesis and progression of human diseases has received increasing attention recently[58,59]. Our enrichment analysis and immunological findings revealed GLS expression might regulate cytokine- and chemokine-related pathways in the TME. A recent study has unveiled GLS blockade downregulated IL-10 production by suppressing mTOR activation[60]. Combined inhibition of several key metabolic enzymes, including GLS, also downregulated the expression levels of multiple chemokines and growth factors related to colon cancer[61]. Hence, blocking GLS may be greatly beneficial for the reversal of the pro-cancer inflammatory microenvironment. Overall, these potential pathways were likely to explain the carcinogenic mechanism of GLS and contribute to underlying therapeutic targets.

On a cautionary note, our research still has certain limitations. Firstly, our study lacks experimental investigations on the specific carcinogenic mechanisms of GLS in the TME. Secondly, the underlying mechanisms of GLS on cuproptosis still require further exploration. Thirdly, further investigations in vivo and in vitro will be conducted in the following work to clarify whether the TME and immune response are altered through targeting GLS in multiple cancers.

Conclusion

In conclusion, GLS is an underlying biomarker for tumor progression, prognosis, conventional antitumor therapy, and immunotherapy, which is beneficial for the identification of suitable patients to formulate individualized and combined treatment strategies. However, since we don't yet know enough about the biological functions of GLS, there is still a long way to go to achieve its therapeutic goals and clinical translation. Meanwhile, further drug development and related clinical trials need to be put on the agenda as soon as possible.

Data availability

All data generated or analysed during this study are included in this published article and its Supplementary Information files. Further inquiries can be directed to the corresponding authors.

Received: 31 August 2024; Accepted: 30 December 2024
Published online: 02 January 2025

References

1. Sung, H. et al. Global Cancer statistics 2020: GLOBOCAN estimates of incidence and Mortality Worldwide for 36 cancers in 185 countries. *Cancer J. Clin.* **71**, 209–249. https://doi.org/10.3322/caac.21660 (2021).
2. Graham, T. A. & Sottoriva, A. Measuring cancer evolution from the genome. *J. Pathol.* **241**, 183–191. https://doi.org/10.1002/path.4821 (2017).
3. de Ruiter, J. R., Wessels, L. F. A. & Jonkers, J. Mouse models in the era of large human tumour sequencing studies. *Open. Biology* https://doi.org/10.1098/rsob.180080 (2018).
4. Zugazagoitia, J. et al. Current challenges in Cancer Treatment. *Clin. Ther.* **38**, 1551–1566. https://doi.org/10.1016/j.clinthera.2016.03.026 (2016).
5. Zhang, Y. & Zhang, Z. The history and advances in cancer immunotherapy: understanding the characteristics of tumor-infiltrating immune cells and their therapeutic implications. *Cell Mol. Immunol.* **17**, 807–821. https://doi.org/10.1038/s41423-020-0488-6 (2020).
6. Matés, J. M., Campos-Sandoval, J. A., Santos-Jiménez, J. L. & Márquez, J. Dysregulation of glutaminase and glutamine synthetase in cancer. *Cancer Lett.* **467**, 29–39. https://doi.org/10.1016/j.canlet.2019.09.011 (2019).
7. Zhu, L., Zhu, X. & Wu, Y. Effects of Glucose Metabolism, Lipid Metabolism, and Glutamine Metabolism on Tumor Microenvironment and Clinical Implications. *Biomolecules* 12, (2022). https://doi.org/10.3390/biom12040580
8. Yang, L., Venneti, S., Nagrath, D. & Glutaminolysis A Hallmark of Cancer Metabolism. *Annu. Rev. Biomed. Eng.* **19**, 163–194. https://doi.org/10.1146/annurev-bioeng-071516-044546 (2017).
9. Altman, B. J., Stine, Z. E. & Dang, C. V. From Krebs to clinic: glutamine metabolism to cancer therapy. *Nat. Rev. Cancer.* **16**, 619–634. https://doi.org/10.1038/nrc.2016.71 (2016).
10. Matés, J. M., Campos-Sandoval, J. A., de Los Santos-Jiménez, J. & Márquez, J. Glutaminases regulate glutathione and oxidative stress in cancer. *Arch. Toxicol.* **94**, 2603–2623. https://doi.org/10.1007/s00204-020-02838-8 (2020).
11. Wu, C., Chen, L., Jin, S. & Li, H. Glutaminase inhibitors: a patent review. *Expert Opin. Ther. Pat.* **28**, 823–835. https://doi.org/10.1080/13543776.2018.1530759 (2018).
12. Xu, L. et al. A glutaminase isoform switch drives therapeutic resistance and disease progression of prostate cancer. *Proc. Natl. Acad. Sci. U.S.A* https://doi.org/10.1073/pnas.2012748118 (2021).
13. Katt, W. P. & Cerione, R. A. Glutaminase regulation in cancer cells: a druggable chain of events. *Drug Discovery Today*. **19**, 450–457. https://doi.org/10.1016/j.drudis.2013.10.008 (2014).
14. Cluntun, A. A., Lukey, M. J., Cerione, R. A. & Locasale, J. W. Glutamine metabolism in Cancer: understanding the heterogeneity. *Trends cancer*. **3**, 169–180. https://doi.org/10.1016/j.trecan.2017.01.005 (2017).
15. Curthoys, N. P. & Watford, M. Regulation of glutaminase activity and glutamine metabolism. *Annu. Rev. Nutr.* **15**, 133–159. https://doi.org/10.1146/annurev.nu.15.070195.001025 (1995).
16. Ding, L. et al. Glutaminase in microglia: a novel regulator of neuroinflammation. *Brain. Behav. Immun.* **92**, 139–156. https://doi.org/10.1016/j.bbi.2020.11.038 (2021).
17. Tsvetkov, P. et al. Copper induces cell death by targeting lipoylated TCA cycle proteins. *Sci. (New York N Y)*. **375**, 1254–1261. https://doi.org/10.1126/science.abf0529 (2022).
18. Rath, S. et al. MitoCarta3.0: an updated mitochondrial proteome now with sub-organelle localization and pathway annotations. *Nucleic Acids Res.* **49**, D1541–d1547. https://doi.org/10.1093/nar/gkaa1011 (2021).

19. Liberzon, A. et al. The Molecular signatures database (MSigDB) hallmark gene set collection. *Cell. Syst.* **1**, 417–425. https://doi.org/10.1016/j.cels.2015.12.004 (2015).
20. Thorsson, V. et al. The Immune Landscape of Cancer. *Immunity* **48**, 812–830e814. https://doi.org/10.1016/j.immuni.2018.03.023 (2018).
21. Krushkal, J. et al. Molecular genomic features associated with in vitro response of the NCI-60 cancer cell line panel to natural products. *Mol. Oncol.* **15**, 381–406. https://doi.org/10.1002/1878-0261.12849 (2021).
22. Bindea, G. et al. Spatiotemporal dynamics of intratumoral immune cells reveal the immune landscape in human cancer. *Immunity* **39**, 782–795. https://doi.org/10.1016/j.immuni.2013.10.003 (2013).
23. Nagarsheth, N., Wicha, M. S. & Zou, W. Chemokines in the cancer microenvironment and their relevance in cancer immunotherapy. *Nat. Rev. Immunol.* **17**, 559–572. https://doi.org/10.1038/nri.2017.49 (2017).
24. Mollica Poeta, V., Massara, M., Capucetti, A. & Bonecchi, R. Chemokines and chemokine receptors: new targets for Cancer Immunotherapy. *Front. Immunol.* **10**, 379. https://doi.org/10.3389/fimmu.2019.00379 (2019).
25. Bule, P., Aguiar, S. I., Aires-Da-Silva, F. & Dias, J. N. R. Chemokine-Directed Tumor Microenvironment Modulation in Cancer Immunotherapy. *Int. J. Mol. Sci.* https://doi.org/10.3390/ijms22189804 (2021).
26. Cao, D. et al. PTEN Expression Was Significantly Associated with PD-L1 score but not with EBV infection in gastric Cancer. *OncoTargets Therapy*. **15**, 1011–1020. https://doi.org/10.2147/ott.S374175 (2022).
27. Masisi, B. K. et al. The role of glutaminase in cancer. *Histopathology* **76**, 498–508. https://doi.org/10.1111/his.14014 (2020).
28. Zhou, W. J. et al. Estrogen inhibits autophagy and promotes growth of endometrial cancer by promoting glutamine metabolism. *Cell. Communication Signaling: CCS* https://doi.org/10.1186/s12964-019-0412-9 (2019).
29. Li, B. et al. Targeting glutaminase 1 attenuates stemness properties in hepatocellular carcinoma by increasing reactive oxygen species and suppressing Wnt/beta-catenin pathway. *EBioMedicine* **39**, 239–254. https://doi.org/10.1016/j.ebiom.2018.11.063 (2019).
30. Xiang, Y. et al. Targeted inhibition of tumor-specific glutaminase diminishes cell-autonomous tumorigenesis. *J. Clin. Investig.* **125**, 2293–2306. https://doi.org/10.1172/jci75836 (2015).
31. Kitayama, K. et al. Pyruvate kinase isozyme M2 and glutaminase might be promising molecular targets for the treatment of gastric cancer. *Cancer Sci.* **108**, 2462–2469. https://doi.org/10.1111/cas.13421 (2017).
32. Draoui, N., de Zeeuw, P. & Carmeliet, P. Angiogenesis revisited from a metabolic perspective: role and therapeutic implications of endothelial cell metabolism. *Open. Biology* https://doi.org/10.1098/rsob.170219 (2017).
33. Huang, H. et al. Role of glutamine and interlinked asparagine metabolism in vessel formation. *EMBO J.* **36**, 2334–2352. https://doi.org/10.15252/embj.201695518 (2017).
34. Takaoka, Y. et al. Mitochondrial pyruvate carrier 1 expression controls cancer epithelial-mesenchymal transition and radioresistance. *Cancer Sci.* **110**, 1331–1339. https://doi.org/10.1111/cas.13980 (2019).
35. Kamarajan, P. et al. Head and Neck squamous cell Carcinoma Metabolism draws on Glutaminolysis, and stemness is specifically regulated by Glutaminolysis via Aldehyde dehydrogenase. *J. Proteome Res.* **16**, 1315–1326. https://doi.org/10.1021/acs.jproteome.6b00936 (2017).
36. Xiao, Y. & Yu, D. Tumor microenvironment as a therapeutic target in cancer. *Pharmacol. Ther.* https://doi.org/10.1016/j.pharmthera.2020.107753 (2021).
37. Wu, T. & Dai, Y. Tumor microenvironment and therapeutic response. *Cancer Lett.* **387**, 61–68. https://doi.org/10.1016/j.canlet.2016.01.043 (2017).
38. Bader, J. E., Voss, K. & Rathmell, J. C. Targeting metabolism to improve the Tumor Microenvironment for Cancer Immunotherapy. *Mol. Cell.* **78**, 1019–1033. https://doi.org/10.1016/j.molcel.2020.05.034 (2020).
39. Wang, B., Pei, J., Xu, S., Liu, J. & Yu, J. A glutamine tug-of-war between cancer and immune cells: recent advances in unraveling the ongoing battle. *J. Experimental Clin. cancer Research: CR.* **43**, 74. https://doi.org/10.1186/s13046-024-02994-0 (2024).
40. Leone, R. D. et al. Glutamine blockade induces divergent metabolic programs to overcome tumor immune evasion. *Sci. (New York N Y).* **366**, 1013–1021. https://doi.org/10.1126/science.aav2588 (2019).
41. DeBerardinis, R. J. Tumor Microenvironment, Metabolism, and Immunotherapy. *N. Engl. J. Med.* **382**, 869–871. https://doi.org/10.1056/NEJMcibr1914890 (2020).
42. Edwards, D. N. et al. Selective glutamine metabolism inhibition in tumor cells improves antitumor T lymphocyte activity in triple-negative breast cancer. *J. Clin. Investig.* https://doi.org/10.1172/jci140100 (2021).
43. Varghese, S. et al. The glutaminase inhibitor CB-839 (Telaglenastat) enhances the Antimelanoma activity of T-Cell-mediated immunotherapies. *Mol. Cancer Ther.* **20**, 500–511. https://doi.org/10.1158/1535-7163.Mct-20-0430 (2021).
44. Li, D. et al. The roles of epigallocatechin gallate in the tumor microenvironment, metabolic reprogramming, and immunotherapy. *Front. Immunol.* https://doi.org/10.3389/fimmu.2024.1331641 (2024).
45. Yang, W. H., Qiu, Y., Stamatatos, O., Janowitz, T. & Lukey, M. J. Enhancing the efficacy of glutamine metabolism inhibitors in Cancer Therapy. *Trends cancer*. **7**, 790–804. https://doi.org/10.1016/j.trecan.2021.04.003 (2021).
46. Ho, W. J. & Jaffee, E. M. Disrupting a converging metabolic target turns up the immunologic-heat in pancreatic tumors. *J. Clin. Investig.* **130**, 71–73. https://doi.org/10.1172/jci133685 (2020).
47. Sharma, N. S. et al. Targeting tumor-intrinsic hexosamine biosynthesis sensitizes pancreatic cancer to anti-PD1 therapy. *J. Clin. Investig.* **130**, 451–465. https://doi.org/10.1172/jci127515 (2020).
48. Qiu, H. et al. Amino acid metabolism in tumor: new shine in the fog? *Clinical nutrition (Edinburgh. Scotland)* **42**, 1521–1530. https://doi.org/10.1016/j.clnu.2023.06.011 (2023).
49. Wang, J. J. et al. A Combination of Glutaminase Inhibitor 968 and PD-L1 Blockade Boosts the Immune Response against Ovarian Cancer. *Biomolecules* 11, (2021). https://doi.org/10.3390/biom11121749
50. Johnson, M. O. et al. Distinct regulation of Th17 and Th1 cell differentiation by glutaminase-dependent metabolism. *Cell* **175**, 1780–1795e1719. https://doi.org/10.1016/j.cell.2018.10.001 (2018).
51. Wang, Q. et al. Targeting metabolic reprogramming in hepatocellular carcinoma to overcome therapeutic resistance: a comprehensive review. *Biomed. Pharmacotherapy = Biomedecine Pharmacotherapie*. **170**, 116021. https://doi.org/10.1016/j.biopha.2023.116021 (2024).
52. Xiao-Yan, W., Xiao-Xia, Y., Peng-Fei, S., Zong-Xue, Z. & Xiu-Li, G. Metabolic reprogramming of glutamine involved in tumorigenesis, multidrug resistance and tumor immunity. *Eur. J. Pharmacol.* **940**, 175323. https://doi.org/10.1016/j.ejphar.2022.175323 (2023).
53. Tanaka, K. et al. Compensatory glutamine metabolism promotes glioblastoma resistance to mTOR inhibitor treatment. *J. Clin. Investig.* **125**, 1591–1602. https://doi.org/10.1172/jci78239 (2015).
54. Sappington, D. R. et al. Glutamine drives glutathione synthesis and contributes to radiation sensitivity of A549 and H460 lung cancer cell lines. *Biochim. Biophys. Acta*. **1860**, 836–843. https://doi.org/10.1016/j.bbagen.2016.01.021 (2016).
55. Sitthideatphaiboon, P. et al. STK11/LKB1 mutations in NSCLC Are Associated with KEAP1/NRF2-Dependent Radiotherapy Resistance Targetable by Glutaminase Inhibition. *Clin. cancer Research: Official J. Am. Association Cancer Res.* **27**, 1720–1733. https://doi.org/10.1158/1078-0432.Ccr-20-2859 (2021).
56. Su, C. et al. Targeting glutamine metabolism through glutaminase inhibition suppresses cell proliferation and progression in nasopharyngeal carcinoma. *Anticancer Agents Med. Chem.* https://doi.org/10.2174/1871520623666230727104825 (2023).
57. Yuan, L. et al. Glutamine promotes ovarian cancer cell proliferation through the mTOR/S6 pathway. *Endocr. Relat. Cancer*. **22**, 577–591. https://doi.org/10.1530/erc-15-0192 (2015).

58. Wang, Z., Chen, H., Peng, L., He, Y. & Zhang, X. Revealing a potential necroptosis-related axis (RP11-138A9.1/hsa-miR-98-5p/ZBP1) in periodontitis by construction of the ceRNA network. *J. Periodontal Res.* **58**, 968–985. https://doi.org/10.1111/jre.13157 (2023).
59. Chen, H. et al. Pyroptosis may play a crucial role in modifications of the immune microenvironment in periodontitis. *J. Periodontal Res.* **57**, 977–990. https://doi.org/10.1111/jre.13035 (2022).
60. Mielle, J. et al. Glutamine promotes the generation of B10(+) cells via the mTOR/GSK3 pathway. *Eur. J. Immunol.* **52**, 418–430. https://doi.org/10.1002/eji.202149387 (2022).
61. Schcolnik-Cabrera, A. et al. A combination of inhibitors of glycolysis, glutaminolysis and de novo fatty acid synthesis decrease the expression of chemokines in human colon cancer cells. *Oncol. Lett.* **18**, 6909–6916. https://doi.org/10.3892/ol.2019.11008 (2019).

Author contributions

D.L.: Data curation, Visualization, Conceptualization, Investigation, Writing – original draft; D.C.: Conceptualization, Data curation, Methodology, Writing – review & editing; Y.Z. and X.Y.: Investigation, Visualization, Writing – review & editing; Y.W. and Z.J.: Formal analysis, Investigation, Writing – review & editing; J.J. and X.C.: Writing – review & editing, Conceptualization, Funding acquisition, Project administration.

Funding

This work was supported by grants from National Natural Science Foundation of China (82373664) and Scientific and Technological Development program of Jilin Province (20240402015GH, 20210101333JC).

Declarations

Competing interests

The authors declare no competing interests.

Additional information

Supplementary Information The online version contains supplementary material available at https://doi.org/10.1038/s41598-024-84916-w.

Correspondence and requests for materials should be addressed to J.J. or X.C.